Validation of the 20th Century Reanalysis for the Northern Hemisphere using Spatial Degrees of Freedom

Martha Dellar

(1044833)

Supervisors: Martin Widmann & Jonathan Eden

MSc Applied Meteorology & Climatology

2010

ABSTRACT

Degrees of freedom (dof) are calculated for the Northern Hemisphere (NH) for the 20th Century reanalysis and for the ERA-40 reanalysis on a month-by-month basis using two different formulae; one based on eigenvalues and the other on statistical moments. Dof are calculated for both temperature and geopotential height for varying time periods, temporal resolutions, latitude bands, zonal regions and pressure levels. Dof are also calculated for the HadSLP2 gridded sea-level pressure dataset. Finally the first six empirical orthogonal functions (EOFs) for January and July are plotted for both the 20th Century reanalysis and ERA-40. An annual cycle was found of a peak in July, medium values in winter and low values in spring and autumn when using both a 6-hourly and a daily resolution. The 20th Century reanalysis matched ERA-40 most closely during winter and it represented geopotential height better than it did temperature. It was found that large-scale dynamics dominated the wintertime variability whilst local processes were more prominent in the summer months. Of the three datasets, ERA-40 had the most dof, followed by HadSLP2 and then the 20th Century reanalysis.

CONTENTS

LIST OF TABLES

LIST OF FIGURES

ABBREVIATIONS

20CR: 20th Century Reanalysis

Dof: Degrees of freedom

ECMWF: European Centre for Medium-Range Weather Forecasts

EnKF: Ensemble Kalman Filter

EnSRF: Ensemble Square Root Filter

EOF: Empirical Orthogonal Function

ESDOF: Effective number of Spatial Degrees of Freedom

GCM: General Circulation Model

IPCC: Intergovernmental Panel on Climate Change

NAO: North Atlantic Oscillation

NCAR: National Center for Atmospheric Research

NCEP: National Centers for Environmental Prediction

NH: Northern Hemisphere

NOAA: National Oceanic and Atmospheric Administration

PNA: Pacific North-American teleconnection pattern

SH: Southern Hemisphere

SLP: Sea-Level Pressure

Introduction

1.1 - Introduction

The 20th Century reanalysis (20CR) was released very recently (January 2010) and as such little research has been carried out using it. Unlike previous reanalyses, the 20CR only uses observations of surface pressure (see section 2.2 for more details), and so a comparison between this and other reanalyses could yield valuable information as to how effective this reanalysis method is. This project aims to investigate the degrees of freedom (dof) in the 20CR for temperature and geopotential height data for the Northern Hemisphere (NH) and to compare these to the dof in ERA-40 and in gridded data as a means of validating the 20CR. It was decided to consider only the NH since there are fewer observations available for the Southern Hemisphere (SH) and thus there is likely to be a difference in skill level between the two hemispheres; this suggests that considering them separately is necessary. The NH was chosen since previous research (see section 2.3) has shown that ERA-40 has a lower error for the NH and since this is to be used as a comparison in this study it was decided that using it for the area where it is most accurate would be ideal.

Compo et al. (2008) state that 'long-term climate datasets are critical to understand the causes of climate variability, to assess its potential predictability, and to evaluate its simulation in climate models'. They mention how such datasets are invaluable to the Intergovernmental Panel on Climate Change (IPCC) to evaluate the variability in their current simulations and to contribute to model improvement. But these are only valid uses if the validity of the dataset itself is known, and this is what this project aims to determine. Uppala et al. (2004) state that 'The uses of ERA-40 reanalyses already extend from studies on bird migration to the detection of climatic temperature trends and to studies of seasonal variations of climate and

their better prediction'; the 20CR will presumably have a similarly large range of applications and as such this project will be of use to all those conducting research in this field.

Given the extensive amounts of validation that ERA-40 had already undergone and its excellent performance in these tests (see section 2.3), it will be taken as truth for the purposes of this study. Thus dof in the 20CR will be measured against those in ERA-40 and an assessment as to the validity of the 20CR will be drawn from this comparison. The comparison with gridded data is to assess how reanalysed data compares with observational data.

This study will include a comprehensive analysis of atmospheric dof. While previous research has compared summer and wintertime dof on varying spatial scales (see section 2.4), to the authors knowledge no previous study has compared dof for varying latitudes or zonal locations. This will be undertaken in this research, as well as comparing dof for multiple temporal resolutions and pressure levels. For each dataset dof will also be calculated on a decade-by-decade basis to see how the reanalyses improve over time. It is assumed that a higher number of dof indicates that more atmospheric processes are resolved in a dataset and thus that it provides a better representation of the atmosphere. It should however be kept in mind that there may be more processes represented in the data than exist in reality, since the model used in the reanalysis process is bound to certain constraints which can cause it to generate additional modes (Fraedrich et al. 1995).

1.2 – Aim

To assess the validity of the 20CR in the NH by comparing its dof with those in the ERA-40 reanalysis and in gridded SLP data.

1.3 – Objectives

1. Calculate dof for the NH in the 20CR and ERA-40 for temperature and geopotential height on a decade-by-decade basis
2. Calculate dof for the NH in the 20CR and ERA-40 for temperature and geopotential height using 6-hourly, daily and monthly resolutions
3. Calculate dof for the NH in the 20CR and ERA-40 for temperature and geopotential height over different spatial areas (latitude bands and zonal regions) and on different pressure levels
4. Calculate dof for the NH in a gridded sea-level pressure dataset and compare with the dof in the 20CR and ERA-40
5. Identify the dominant trends for the NH in the temperature and geopotential height data in each of the 20CR and ERA-40 using EOF analysis

1.4 - Dissertation Organisation

This dissertation is organised into six chapters. The second is a review of literature pertaining to the 20CR, ERA-40, previous studies investigating atmospheric dof and research concerned with the parameters to be varied in this study. Chapter 3 gives details of the datasets used and the methods employed in this research. Chapter 4 includes the results found in this study organised according to the objectives and these are discussed in chapter 5.

Finally, chapter 6 lists the key findings from this investigation, as well as its limitations, and gives suggestions for further research.

Literature Review

2.1 – Introduction

This literature review is divided into four main sections. The first (2.2) is a detailed study of the 20CR itself and considers the mechanics of the data assimilation process. The second section (2.3) reviews previous validation studies on ERA-40. The third section (2.4) details past research on atmospheric degrees of freedom and the fourth section (2.5) considers each of the parameters to be varied in this study and reviews the literature relating to these. Finally there is a summary (2.6) relating each of these areas to the overall aim of this research.

2.2 - Twentieth Century Reanalysis

Data assimilation is a process 'in which observations distributed in time are merged together with a dynamical numerical model of the flow in order to determine as accurately as possible the state of the atmosphere' (Talagrand 1997). Data assimilation is used to perform atmospheric reanalyses and is an incredibly useful tool since it can produce complete long-term climatological datasets, despite the fact that there may be missing data over some areas and for some time periods.

For the 20CR, the empirical data used consists entirely of surface pressure observations (Compo et al. 2008), distinguishing it from other long-term reanalysis efforts to date. The use of a single variable is described by Toth (1995) as *temporal embedding* (as opposed to *spatial embedding* which uses multiple variables) and has the advantage of requiring relatively small amounts of data. Toth describes the theory of temporal embedding as guaranteeing 'that the phase space of a dynamical system can be reconstructed, with very few exceptions, from a single-state variable'. Surface pressure was selected as the variable of choice since of all the data available for the

early twentieth century, it was surface pressure that was the most widely available and was considered to be the most reliable. It is also possible to extrapolate more information about the state of the free troposphere from surface pressure readings than it is from observations of e.g. surface wind or temperature (Whitaker et al. 2004, Compo et al. 2006).

The data assimilation method used is a variation of the Ensemble Kalman Filter (EnKF) known as the Ensemble Square Root Filter (EnSRF) (Whitaker and Hamill 2002). Ensemble filters 'are often easier to implement than most traditional data assimilation methods' (Anderson et al. 2005) and in a study conducted by Compo et al. (2006) it was found that an ensemble filter performed better than other data assimilation methods when analysing surface pressure data for a limited number of observations.

The traditional EnKF first runs a model simulation to determine background conditions, $\boldsymbol{x^b}$ (having m dimensions). From this the m x m background error covariance matrix, $\boldsymbol{P^b}$, can be determined. The covariance matrix is defined as follows:

$$C = \begin{pmatrix} c_{11} & c_{12} & \dots & c_{1n} \\ c_{21} & c_{22} & & \vdots \\ \vdots & & \ddots & \vdots \\ c_{n1} & \dots & \dots & c_{nn} \end{pmatrix} \qquad \textbf{[2.2.1]}$$

where $c_{ij} = \frac{1}{T-1}\sum_{k=1}^{T}(x_i(t_k) - \overline{x_i})\left(x_j(t_k) - \overline{x_j}\right)$

n is the number of gridcells and T is the number of timesteps (Widmann 2010).

The process of establishing these background parameters is known as the *forecast* stage; once this is achieved we can progress to the *analysis* stage. This produces an

analysed parameter $\boldsymbol{x^a}$ which includes both the simulated conditions and the effect of observations. It is given by the Kalman filter update equation:

$$\boldsymbol{x^a = x^b + K\left(y^o - Hx^b\right)} \quad \textbf{[2.2.2]}$$

where

$$\boldsymbol{K = P^b H^T \left(HP^b H^T + R\right)^{-1}} \quad \textbf{[2.2.3]}$$

and $\boldsymbol{H}$ is the operator that 'converts the model state to the observation space' (Whitaker and Hamill 2002), i.e. it gives the simulated value of surface pressure at the observation locations; $\boldsymbol{y^o}$ is the set of observations (with p dimensions) and $\boldsymbol{R}$ is the p x p observation error covariance matrix. The analysis error covariance is given by $\boldsymbol{P^a}$:

$$\boldsymbol{P^a = (I - KH)P^b} \quad \textbf{[2.2.4]}$$

These equations can be written in terms of the ensemble mean (denoted by a bar) and the deviation from the mean (denoted by a prime):

$$\boldsymbol{\overline{x}^a = \overline{x}^b + K\left(\overline{y}^o - H\overline{x}^b\right)} \quad \textbf{[2.2.5]}$$

$$\boldsymbol{x'^a = x'^b + K\left(y'^o - Hx'^b\right)} \quad \textbf{[2.2.6]}$$

(Whitaker and Hamill 2002)

The EnKF has a tendency to systematically underestimate $\boldsymbol{P^a}$ (Whitaker and Hamill 2002, Whitaker et al. 2004, Anderson et al. 2005) which can lead to filter divergence. This means that 'the ensemble progressively ignores observational data more and more in successive cycles, leading to a useless ensemble' (Hamill and Whitaker 2001). To account for this in the 20CR, 'the background error covariances are inflated in amplitude and localized in space' (Compo et al. 2006).

Previously a response to the issue of filter divergence was to use perturbed observations, though this tended to cause errors in the observation error covariances.

The EnSRF does not require the use of perturbed observations and has been shown to be less susceptible to filter divergence than the EnKF (Whitaker and Hamill 2002). In this case equation [2.2.5] remains the same but equation [2.2.6] becomes:

$$\boldsymbol{x'^a = x'^b - \widetilde{K} H x'^b} \qquad \textbf{[2.2.7]}$$

where

$$\boldsymbol{\widetilde{K} = P^b H^T \left[\left(\sqrt{HP^b H^T + R}\right)^{-1}\right]^T \times \left[\sqrt{(HP^b H^T + R)} + \sqrt{R}\right]^{-1}} \qquad \textbf{[2.2.8]}$$

(Whitaker and Hamill 2002)

This involves calculating the square roots of matrices, which are both non-unique and computationally demanding. However, if $\boldsymbol{R}$ is diagonal (i.e. if the observation errors are uncorrelated) then 'observations may be processed one at a time, and the EnSRF requires no more computation than the traditional EnKF with perturbed observations' (Whitaker and Hamill 2002). For the 20CR it is assumed that the observation errors are uncorrelated and so the observations are processed sequentially (Compo et al. 2008). Once $\boldsymbol{x^a}$ has been found for one observation it becomes the $\boldsymbol{x^b}$ for the next observation.

2.3 - ERA-40

It is widely agreed that ERA-40 is an improvement on those reanalyses which preceded it (Santer et al. 2004, Uppala et al. 2004 & 2005, Ma et al. 2008). Santer et al. (2004) identify it as having a higher signal to noise ratio than NCEP-50 (aka NCEP-2) and Uppala et al. (2005) compare ERA-40 5-day forecast scores with those presented by Kistler et al. (1991) for the NCEP/NCAR reanalysis and find that 'the correlations from ERA-40 are about 10 percentage points higher than from NCEP/NCAR for the northern hemisphere'. Uppala et al. (2005) also found that over the entire ERA-40 period, the detection rate for tropical cyclones in the NH is never below 93% and that its storm-tracking facilities are an improvement over ERA-15.

Here are plots showing the root-mean-square errors of the background forecast and the analysis fits to 500hPa radiosonde temperatures:

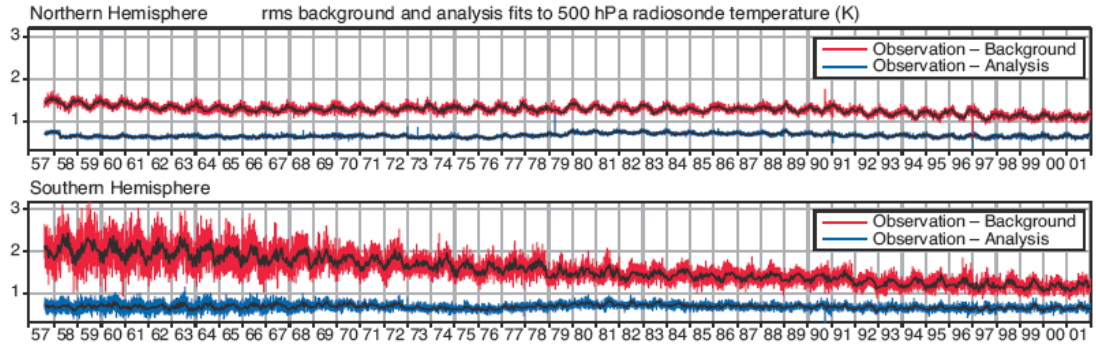

Fig 2.3.1: Root-mean-square ERA-40 background (daily (red) and 15-day moving average (black)) and analysis (daily (blue) and 15-day moving average (black)) fits to 500hPa radiosonde temperature observations over the extratropical Northern (upper) and Southern (lower) Hemispheres.

Source: Uppala et al. (2004)

The evidence of improvements to the observing system can be clearly seen for the SH plot as both the error and variability in the background fit decrease. Errors in the

analysis fit are fairly constant, though there is more variability towards the beginning of the period for the SH; this will be due to the large background errors for this time. There is a slight increase in the analysis fit in the 1980s for both hemispheres. This is because as well as matching radiosonde data, the analysis also had to match satellite radiance data for these years (Uppala et al. 2004).

There are also aspects of the climate system which ERA-40 does not represent so accurately. For instance, Uppala et al. (2005) describe how it produces 'excessive precipitation over tropical oceans and a too strong Brewer-Dobson circulation'; they also find that the analysis fit to observations is less good when there is a strong El Niño event in progress. Uppala at al. (2004) find that ERA-40 has a poor all-sky radiation budget due to the radiative properties of clouds being poorly simulated. Santer et al. (2004) describe how it prescribes 'unrealistically large stratospheric warming in the mid-1970s' as well as having a cold bias in the tropics at around 100hPa in the early 1980s. Finally, Bengtsson et al. (2004) investigated the possibility of using ERA-40 to study long-term climate trends, but concluded that such trends were distorted by changes to the observation network and that ERA-40 had a tendency to produce artificial trends due to the nature of the observing system.

2.4 - Degrees of Freedom Literature Review

The number of dof in the atmospheric system can be viewed as the dimensionality of the atmosphere (Toth 1995). That is the number of independent systems required to generate the same level of complexity as that which exists in the atmosphere. The concept of dof is related to that of the χ^2 distribution which can be defined as follows:

If a_1, a_2, … , a_k are independent standard normal random variables, then the random variable

$X=a_1^2 + a_2^2+\ldots+a_k^2$ *is said to have a χ^2 distribution with k degrees of freedom.*

(Hazelrigg 2004)

Thus Bretherton et al. (1999) define the dof *N**of a time-varying spatial field $\psi(t)$ as 'the number of uncorrelated random normal variables a_k, each having zero mean and the same population variance $\langle a^2 \rangle$, for which the χ^2 distribution for the specified functional $[\sum_{i=1}^{N} \psi_i^2(t)$, N is number of stations] most closely matches the PDF [probability density function] of the functional of $\psi(t)$.' Toth (1995) calls attention to the fact that the data sets used in studies of atmospheric dimensionality are not able to identify small-scale processes, and thus 'the number of dof in a dataset is not necessarily the dimension of the underlying object' (Toth 1995). Instead he describes estimates of the dof as 'the dimension of a hypothetical subsystem of the atmosphere that governs the large scale flow'.

There have been a number of studies concerned with the estimation of the dof of atmospheric circulation. Unfortunately, there is no simple direct comparison to be made since the concept of

dof is not uniquely defined and different calculation methods can produce widely varying results. One of the earliest studies in this area was performed by Edward Lorenz (1969), for which he used NH twice-daily data over a period of five years and on three pressure levels over a grid of 1003 points. 'He computed a mean square type distance between all possible pairs of circulation patterns in his data base' and 'assumed that the difference between two patterns at each grid point follows a normal distribution' (Toth 1995). Lorenz assumed that the averaged sum of the square of these differences (i.e. the mean-square error) follows a χ^2 distribution. He then compared the distribution of the mean-squared errors from his wintertime empirical data with χ^2 distributions of varying dof. He found that the closest match came when the number of dof was equal to 44, and so concluded that his wintertime data contained approximately 44 dof (Lorenz 1969).

In 1983 Livezey and Chen undertook a study on field significance, which included consideration of dof. Their method used the binomial distribution and involved calculating the ratio of the number of successful Bernoulli trials to the number of spatial points. The number of dof is equal to the number of independent trials (Wang & Shen 1999); this involves running a series Monte Carlo simulations. They found that for the NH at the 700hPa level there were approximately 55 dof in summer and 35 in winter (Livezey& Chen 1983).

Horel performed a study in 1985 examining the persistence on the 500hPa height field during winter in the NH. He used a technique involving pattern correlation and defined the dof to be the number of statistically independent gridpoints. He found that 'for the case of the unfiltered data, roughly 30 gridpoints are statistically independent; if wavenumbers greater than 4 are removed,

then only 20 gridpoints are distinct statistically from one another' (Horel 1985). He attributed these low numbers to the large spatial scale of persistent episodes.

Van Den Dool and Chervin (1986) compared the persistence of anomalies in a general circulation model and in the Earth's atmosphere. As a by-product of this they calculated the dof for monthly mean anomaly height fields. Their method involved estimating the dof using the standard deviation of a pattern correlation coefficient. They found that for the area north of 20°N, the number of wintertime dof ranged from 15 to 20 and for summertime was around 40. They concluded that such low values implied a 'large spatial extension of height anomalies at all levels' (Van Den Dool and Chervin 1986).

In 1995 Fraedrich et al. used a generalised version of Lorenz's method to calculate the dof in the monthly mean anomalies of the 1000hPa height field for NH mid-latitudes and for the Eastern North Atlantic/European sector. They also compared dof in the empirical data to those found in GCM simulations. To calculate the dof they derived the following formula:

$$dof = \frac{N^2}{\sum_{i=1}^{N} \lambda_i^2} \qquad \textbf{[2.4.1]}$$

Where N is the number of variables and λ_i are the eigenvalues of the covariance matrix of the dependent variables (Fraedrich et al. 1995). For NH mid-latitudes they found that using unfiltered data gave a minimum number of dof in February with a value of 25; this increased to a maximum of 37 in July. Using low-pass filtered data reduced the number of dof and using bandpass filtered data increased it. For the Eastern North Atlantic/European sector for unfiltered data they found the minimum value came in February (12) and the maximum in July (15). When comparing dof in the empirical data to those found in model simulations they found that for the

NH the GCM data had approximately 5 degrees of freedom more; also that the maximum shifted from July to August. They account for this increased number of dof by stating that 'the model tends to activate a larger number of its own intrinsic modes to cope with the dynamically required constraints due to the limited number of nonlinear interactions that, otherwise, could create a few structurally stable and active flow regimes' (Fraedrich et al. 1995). That is to say the model produces more modes than actually exist in order to meet its programmed constraints.

Toth (1995) investigated the dof in extratropical NH wintertime circulation patterns using data for the 700hPa height field over a 33 year period. He used two different methods to do this; the first is similar to Lorenz's method and the second he terms the *hyperspheres method* which 'compares the local density properties in the empirical data to density in independently and identically distributed normal distributions with different number of dof' (Toth 1995); the best fit determines the most likely number of dof. It focuses on the smallest scales available and Toth describes it as giving an accurate estimate of dof, without the negative bias that exists for several other calculation methods. For the χ^2 (Lorenz's) method, he calculated that for daily data there were between 23 and 34 dof and for the hyperspheres method he calculated there were 24 dof.

In 1999, Wang and Shen compared four different methods for estimating the spatial dof of a climate field. They considered both hemispheres separately and used data for monthly surface temperatures covering a period of 140 years. The first method is similar to that used by Fraedrich et al. as described above. It was originally devised by North et al in 1982 and instead of calculating a single value it gives bounds for the estimate of the dof; Wang and Shen term this the χ^2 method. They found that 'when the length of data is short, a large sampling error results in

the eigenvalue estimate of covariance matrix, hence, a large error in dof estimation'. They also found that this method tended to systematically underestimate the dof, though they did find that it also produced the lowest standard deviation of the four. The next method they investigated they term the Z method; this uses the variance of the Fisher Z transformed pattern correlation coefficients between two realizations of a field. They found that this worked well so long as the mean and variance of the field did not change with spatial location; otherwise it produced an estimate for the dof with a significant error. The third method is called the S method and defines the dof as the ratio of the variance of the field's average to the average of the variance field. It was found that this was subject to the same problems as the Z method in terms of varying mean and variance with spatial location. The final method is the B method and is the same as that used by Livezey and Chen (1983) as described above. They found that it still worked well for short datasets (though with a fairly large standard deviation) and that it didn't have any issues with the mean and variance varying with spatial location. They concluded that the B method 'provides the most accurate estimate of the dof' (Wang and Shen 1999), though because of the need to run multiple Monte Carlo simulations it does require a significant amount of computing power. Their results for the NH are as follows:

Table 2.4.1: Maximum and minimum dof calculated for the NH in Wang and Shen's (1999) study using different dof formulae

Method	Minimum	Maximum
χ^2	15 (March)	22 (July)
Z	31 (March)	64 (July)
S	17 (March)	39 (November)
B	45 (March)	83 (July)

They found that the χ^2, Z and B methods all had a similar annual cycle, with lower values in winter and higher ones in summer; however the S method was quite different.

Bretherton et al. (1999) devised two formulae for the calculation of the effective number of spatial degrees of freedom (ESDOF). These are:

$$N^*_{mm} = \frac{2\langle E \rangle^2}{var(E)} \quad \textbf{[2.4.2]}$$

$$N^*_{ef} = \frac{\left(\sum_{k=1}^{N} \lambda_k\right)^2}{\sum_{k=1}^{N} \lambda_k^2} \quad \textbf{[2.4.3]}$$

(Bretherton et al. 1999)

Derivations of these formulae and details of the notation used are given in Appendix 1. As Bretherton et al. state: 'N^*_{ef} depends only on the partitioning of the variance between the EOFs', and although it is based on their first formula, it will produce a different result as long as the time series is finite or the ψ_i's [as defined at the beginning of this section] are non-normally distributed. [2.4.3] is similar to the χ^2 method investigated by Wang and Shen (1999) and described above. Bretherton et al. found the same negative bias for N^*_{ef} for short time series as Wang and Shen noted in their study. They are also in agreement about the low standard deviation found in the results for this method. Bretherton et al. also investigated bias and scatter of N^*_{mm} and found that this was the opposite of N^*_{ef} in that it produces results with a very slight positive bias and a large scatter. The difference between the formulae's results for time series of different lengths can be seen below:

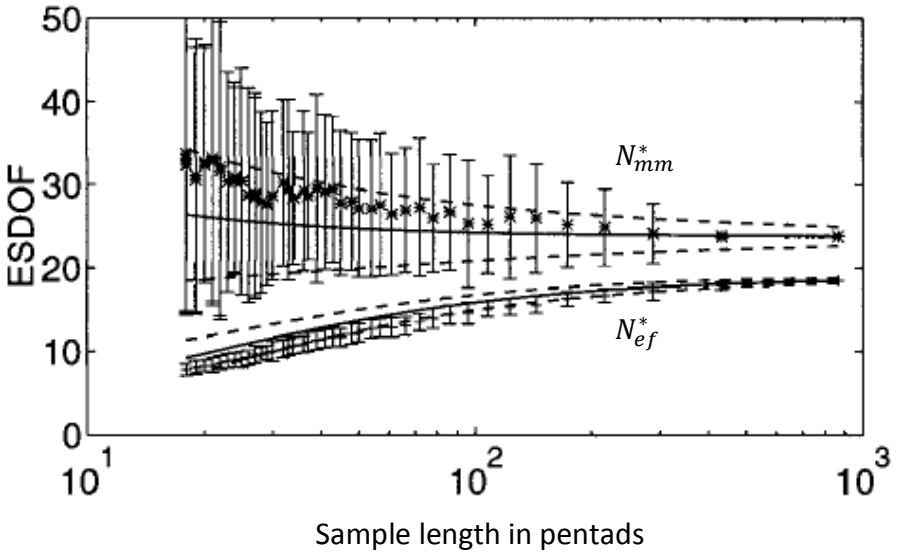

Fig 2.4.1: ESDOF against sampling period. The crosses and error bars denote ensemble means, bracketed by one standard deviation. The solid and dashed lines show the theoretical estimates of the means, bracketed by one standard deviation, of N^*_{mm} and N^*_{ef}. Source: Bretherton et al. (1999)

They estimated dof for the NH wintertime 500hPa height field using data from 48 years. They calculated N^*_{mm} = 24 and N^*_{ef} = 19.

2.5 - Variable Parameters Literature Review

In this study several different parameters will be varied and the dof calculated for each variation. These parameters are decade, temporal resolution, latitude band, zone and pressure level; also each calculation will be performed separately for each month. The effects of varying some of these parameters have been previously investigated and the results of such studies are given below.

Variations by Decade

Compo et al. (2006) investigated the feasibility of a 100-year reanalysis using only surface pressure data. They performed local anomaly correlation between the results of experiments using an EnSRF for 1905 and 1935 for the 700hPa geopotential height field with the full NCEP/NCAR 4-times-daily reanalysis for 2001. They found that for the NH extratropics both the 1905 and 1935 results were very highly correlated with those of the NCEP/NCAR reanalysis and that there was very little difference between the two experimental runs. In contrast, for the tropical regions and the SH the 1935 results were an improvement over those from 1905. They conclude that 'the analysis quality for the Northern Hemisphere extratropics will be consistent throughout the twentieth century, while the quality for the Tropics and Southern Hemisphere will increase with additional observations' (Compo et al. 2006).

Uppala et al. (2004) investigated how the quality of ERA-40 varies with time. They calculated the root-mean-square error between the analysis and observations for both surface pressure and temperature at 500hPa; for surface pressure they used SYNOP and SHIP

observations and for temperature they used radiosonde data. For the NH they found that the error in the surface pressure analysis dropped over the course of the period from a little under 1hPa to a little over 0hPa; they attribute this drop to improvements in the observation network. The error in the analysis of temperature was fairly consistent for the NH over the whole period at around 0.5K.

Temporal Resolutions

Fraedrich et al. (1995) calculated dof for monthly mean anomalies of the 1000hPa height field for NH mid-latitudes, as described in section 2.4. They tried adding bimonthly data and recalculating the dof and found that this had no effect on the results except for a smoothing of the annual cycle. They also found that halving the number of points (in time) had no influence on the number of dof. They attributed this stability of dof estimates to the large sample size used, since this causes the correlation coefficients used in their dof calculations to be relatively stable.

Latitude Bands

Anderson et al. (2005) investigated the assimilation of surface pressure observations using an ensemble filter in an idealized global atmospheric prediction system. They calculated the prior ensemble mean error and found that 'for temperature in the middle of the atmosphere, the largest errors are found in the Tropics'. They also found that within the Tropics the errors have a smaller spatial scale than at higher latitudes.

Pressure Levels

Fraedrich et al. (1995) also calculated dof at different pressure levels. They discovered 'a tendency for dofs to increase with height', though the increase is relatively small with the maximum difference between dof at 300hPa and 1000hPa of unfiltered data being around 4.

Months

All the dof studies previously mentioned in section 2.4 which included a seasonal comparison found that there were more dof in summer than in winter. Fraedrich et al. (1995) attributed this to large-scale dynamics dominating wintertime variability, with local processes such as convection being more prominent in the summer months. This means more independent modes (and thus more dof) in summertime.

The large-scale dynamics discussed by Fraedrich et al. include teleconnection patterns. Wallace et al. (2003) describe how the North Atlantic Oscillation (NAO) and the Pacific North-American pattern (PNA) dominate the wintertime geopotential height field and how they weaken and are obscured by local processes in the summer months.

2.6 – Summary

Section 2.2 (20CR) gives details about the assimilation process used which will be useful in interpreting the results from this study. Section 2.3 (ERA-40) emphasises the high quality of ERA-40 in the NH and reaffirms that that it is appropriate to take it as truth for the purposes of this study. We learn that ERA-40 does not represent precipitation or cloud-cover (and hence other closely related variables) well and so these are not used in this study. Temperature is well represented and so this is one of the variables that is used. Section 2.4 (DOF) shows that there are many different ways of calculating dof, each with associated advantages and disadvantages. If the time-series used is too short this can adversely affect the results, though given the long time periods used in this study this is unlikely to be an issue. All the studies considered which included a seasonal comparison found that dof tend to be higher in summer than winter. Section 2.5 (Variable Parameters) reviewed literature relating to the parameters due to be varied in this study. While some useful results were found it should be noted that there was little literature relating to some of these parameters, particularly in terms of dof. This highlights that there has been little research done on how dof vary with zonal region, latitude, etc. and this study aims to amend this.

Data & Methods

3.1 – Introduction

This chapter has two main sections: Data and Methods. The Data section has three parts, one relating to each dataset, in which key features of the datasets are given. The Methods section has four parts: the first describes the selected dof calculation method; the second explains the necessary alterations made to the datasets before they could be used; the third describes the processes involved for calculating dof for each of the parameters to be varied; and the fourth describes the method used to plot the leading EOFs.

3.2 - Data

3.2.1 - 20th Century Reanalysis

The 20CR was released in January 2010. It is the product of data assimilation, producing a climatological record covering the period 1871 to 2008. It is the result of international cooperation led by the National Oceanic and Atmospheric Administration (NOAA) and uses a 2° lat-lon grid with 6-hourly timesteps. It produces analyses of a large number of variables, including cloud cover, gravity wave stress and potential evaporation rate, as well as more conventional options such as air temperature and geopotential height (NOAA, 2010). Unlike other reanalysis efforts, the 20CR uses only surface pressure observations for its empirical data. This data came from the International Surface Pressure Databank which Compo et al. (2008) describe as 'the most complete data set of pressure observations ever assembled'. It has a total of 1,751,291,205 observations of surface and sea-level pressure from 33,628 stations over the period 1768 – 2008 (Yin et al. 2008). Figure 3.2.1.1 shows how the number of observations varies over this time:

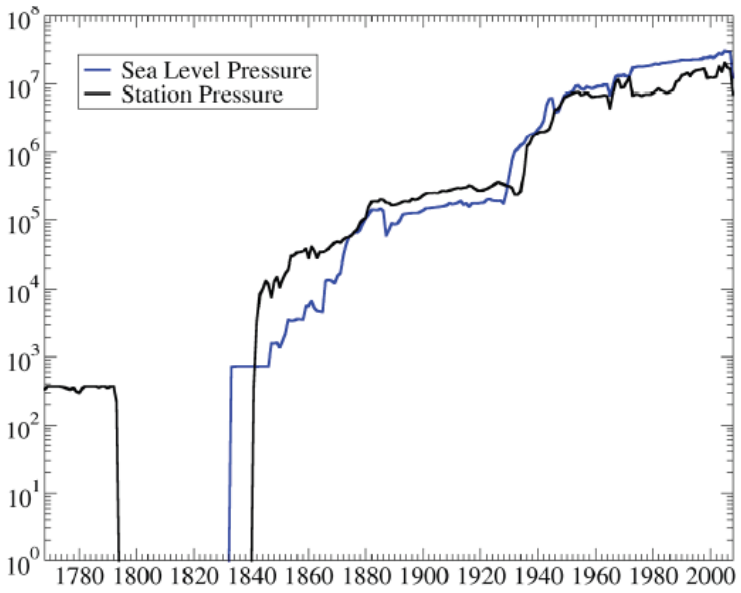

Fig 3.2.1.1: Number of observations used in the 20CR over time. Source: Yin et al. (2008)

The spatial distribution of these observations for the years 1875, 1950 and 2000 can be seen below:

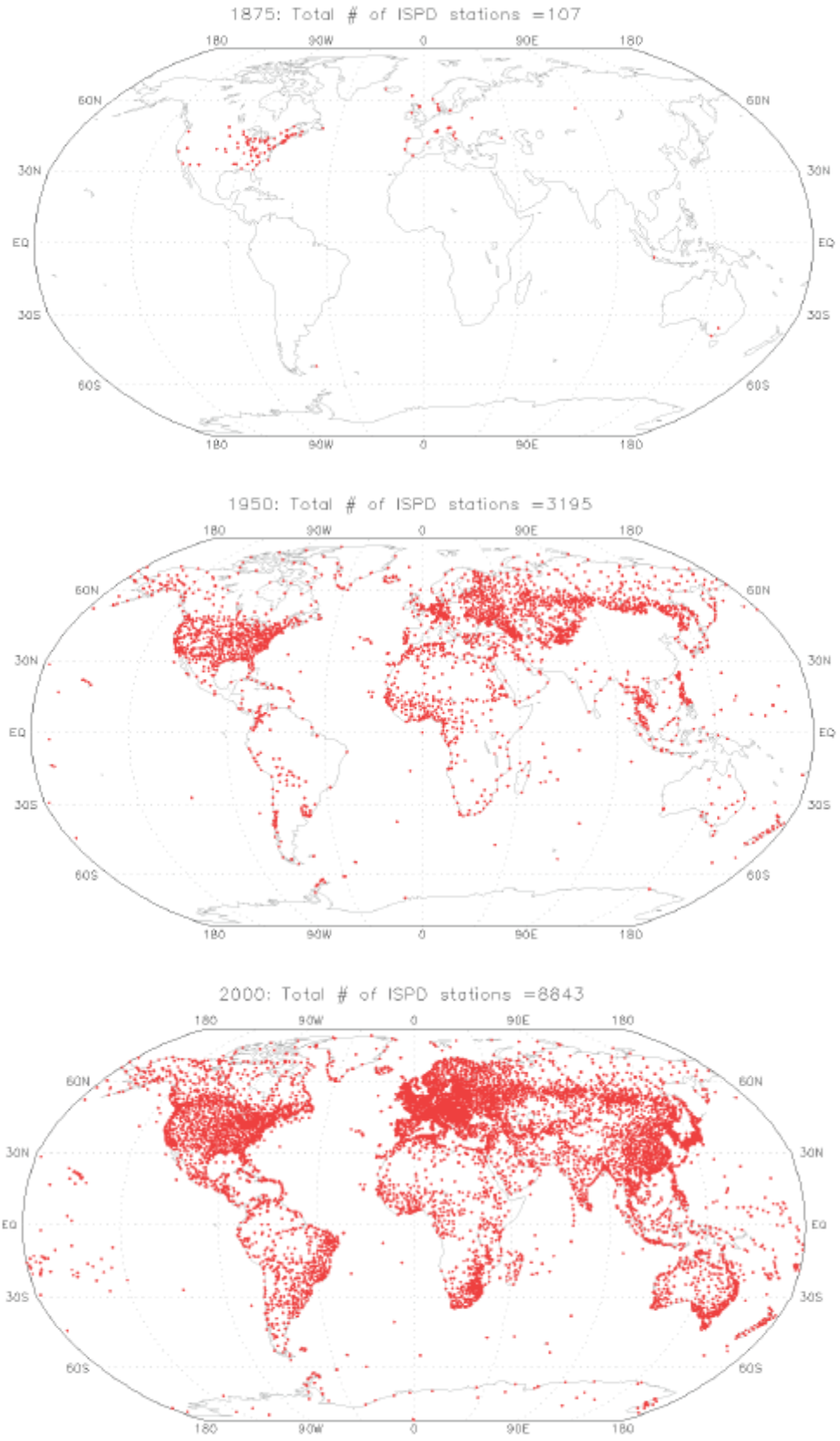

Fig 3.2.1.2: Spatial distribution of observation stations for the 20CR for the years 1875, 1950 and 2000. Source: Yin et al. (2008)

The model used for the 20CR is the atmospheric component of NCEP's operational Climate Forecast System model. This has a spatial resolution of just under 200km on an irregular Gaussian grid in the horizontal and operates on 28 vertical levels, with the top being at 0.2hPa. A 56 member ensemble is run on 9-hour integrations for each step of the reanalysis. The reanalysis process used is the Ensemble Square Root Filter; this is discussed in more detail in section 2.2.

20CR data is provided by the NOAA/OAR/ESRL PSD, Boulder, Colorado, USA, from their website at http://www.esrl.noaa.gov/psd.

3.2.2 - ERA-40

ERA-40 is a reanalysis conducted by the European Centre for Medium-Range Weather Forecasts (ECMWF). It was begun in 2000 and was completed in 2003, having produced a total of 70,000 GB of stored information (Uppala et al. 2004). It covers the span from September 1957 to August 2002 using a 6-hour assimilation period on a 2.5° lat-lon grid. The assimilation method is a variation of 3D-Var and it uses a spectral model with a T159 (~125km) resolution and 60 vertical levels (Uppala et al. 2005). The data assimilation system 'was designed to produce analyses of atmospheric temperature, horizontal winds, humidity and ozone, and a number of surface variables' (Uppala et al. 2005) and indeed the number of variables available is very large, including options such as snowmelt, gravity wave stress and cloud cover.

Unlike the 20CR, ERA-40 uses a variety of different observations, rather than just surface pressure. These include temperature, humidity, ozone and snow depth, to name but a few. The assimilation system also takes account of trends in carbon dioxide, as well as several other radiatively active gases, as detailed by the IPCC (Uppala et al. 2004). This means they use a large variety of observing equipment, including radiosondes, aircraft and satellites. The distribution of radiosonde and surface measurements can be seen below:

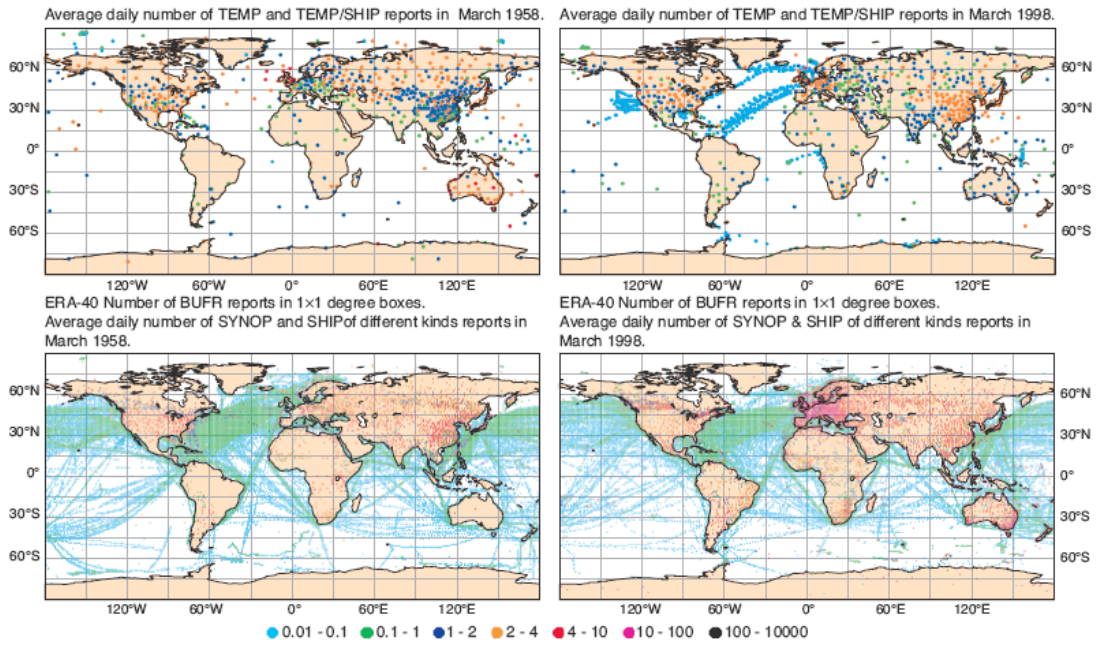

Fig 3.2.2.1: ERA-40 monthly coverage of radiosonde (upper) and surface (lower) observations in 1958 (left-hand panels) and 1998 (right-hand panels). Source: Uppala et al. (2004)

While the number of radiosonde measurements taken decreases towards the end of the period, the number of satellite observations increases steadily from their introduction in 1973 (Uppala et al. 2004). The introduction of satellites was particularly useful for analyses of the SH, which had previously had considerably fewer observations than the NH due to the smaller land area present there. In the pre-satellite era the NH had also benefitted from radiosonde data from ocean weather ships which had not been available for the SH (Uppala et al. 2005). The influence of conventional data (i.e. not from aircraft or satellites) is restricted to the troposphere and lower stratosphere, whilst satellite data is necessary for large ocean areas, polar regions and the upper stratosphere, so it is valuable to use both (Uppala et al. 2004). In the early years of the ERA-40 period there are 'significant gaps in the coverage of synoptic surface data from many countries' (Uppala et al. 2004), which affect the quality of the reanalysis for this time.

As for the 20CR, errors in the observations used in ERA-40 are assumed to be unbiased. This means that it is necessary to correct any systematic errors which may occur. To this end, 'radiosonde temperatures later in the period are corrected and satellite data are bias-tuned'; this is done using the background forecast as a reference (Uppala et al. 2004). It was found that radiosonde errors were 'larger and more variable in time and space' earlier in the period, with many being rejected through quality control tests. This was less of an issue towards the end of the period.

ERA-40 data is provided by ECMWF through the British Atmospheric Data Centre (BADC) from their website at http://badc.nerc.ac.uk/data/ecmwf-e40.

3.2.3 - HadSLP2

The HadSLP2 dataset produced by the Hadley Centre was chosen as the gridded SLP dataset for this study. This covers nearly all the period included in the 20CR (1850-2004) using monthly timesteps on a 5° lat-lon grid. It is a globally-complete dataset and has undergone extensive quality control checks (Allan & Ansell 2006). Validation has been performed on this dataset by comparing it to other datasets, including ERA-40. It was found that 'over regions of high altitude, HadSLP2 and ERA-40 showed consistent differences suggestive of potential biases in the reanalysis model' (Allan & Ansell 2006) and that they were more closely matched in winter than in summer 'because of the greater meteorological signal in this season' (Allan & Ansell 2006). They also found that there was greater disparity in areas where HadSLP2 had fewer observations available. The spatial distribution of observations for this dataset for the period 1991-2000 can be seen below:

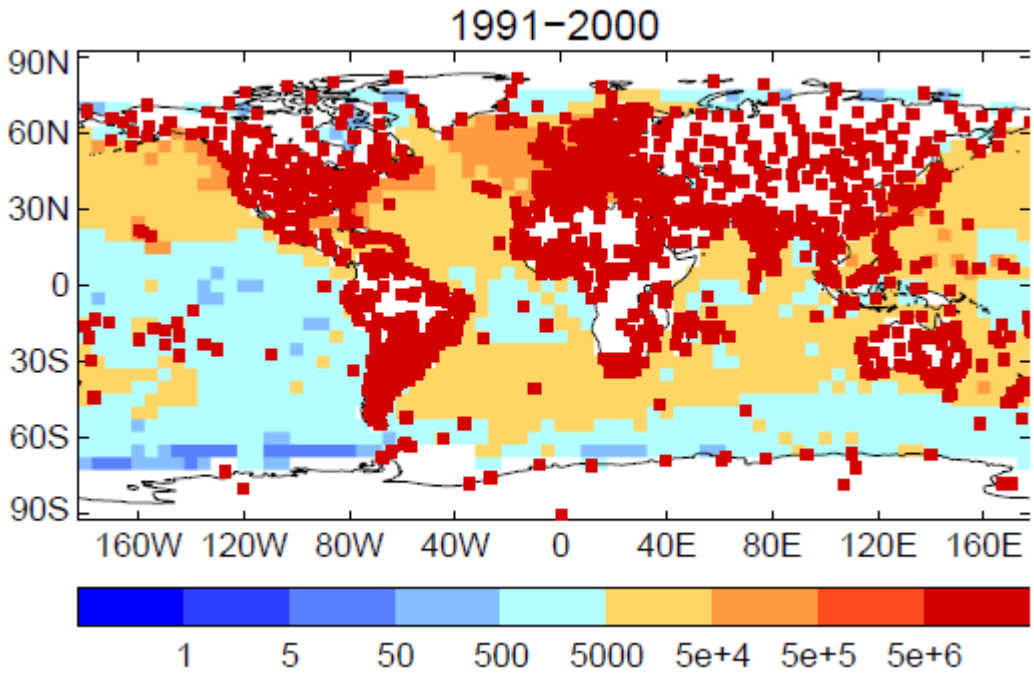

Fig 3.2.3.1: Spatial distribution of HadSLP2 observations for the period 1991-2000. Red squares indicate the location of stations, not the number of observations. Source: Allan & Ansell (2006)

The HadSLP2 dataset is available from the Met Office Hadley Centre website at http://www.hadobs.org. More details can be found in Allan & Ansell (2006).

3.3 - Methods

3.3.1 – Degrees of Freedom

The aim of this research is to assess the validity of the 20CR and it was decided that an effective way to achieve this would be to calculate its dof. Dof was selected as the statistic of choice for this study since it produces a single value describing the complexity of the atmosphere. This simplicity makes it ideal for comparing results from different datasets. Also, as Bretherton et al. (1999) describe: 'The concept of ESDOF is certainly no less clearly defined (in a χ^2 context) and of no less practical value than the number of significant modes in an EOF expansion, yet it seems to be much less widely understood and appreciated in the research community'. As such, this study hopes to raise the profile of spatial dof as an efficient and legitimate method for assessing the validity of a dataset.

There are many different ways of calculating dof, several of which are described in section 2.4. This study will use those employed in Bretherton et al. (1999):

$$N_{mm}^{*} = \frac{2\langle E \rangle^2}{var(E)} \qquad \textbf{[3.3.1.1]}$$

$$N_{ef}^{*} = \frac{\left(\sum_{k=1}^{N} \lambda_k\right)^2}{\sum_{k=1}^{N} \lambda_k^2} \qquad \textbf{[3.3.1.2]}$$

Derivations of these and details of the notation used can be found in Appendix 1. Wang and Shen (1999) criticised a variant of [3.3.1.2] as producing a large error when applied to a short time-series and they highlighted its tendency to systematically underestimate the dof. These accusations also apply to this version but the time series used in this study will be sufficiently long that the error is negligible. Also, by using both of the formulae above, an appropriate

estimate of dof should be possible since they have contrasting tendencies; the first producing a wide spread and low bias and the other producing a low spread with a higher bias.

3.3.2 - Alterations

In order to apply these formulae the datasets for comparison were first re-gridded so that they were all on the same scale as the dataset with the largest sized gridcells. For instance, to compare dof in the 20CR (2° grid) with those in ERA-40 (2.5° grid), the 20CR data was re-gridded to a 2.5° grid. This was done using the 'Regrid' program by M. Widmann (2000). It was decided to upscale the datasets rather than downscale them to the smallest grid-size, as to downscale them would not add any of the additional data expected at the smaller scale that would be present in the dataset that originally had the smallest grid-size; this would give an inaccurate representation of the dof of the scaled data. The 'Regrid' program does not include the area directly around the pole in its output grid and so these cells were removed from the unscaled data to allow for an accurate comparison.

A weighting was also applied to the data based on the latitude of each gridcell. This was to account for the difference in the size of gridcells at different latitudes which could cause the gridcells around the pole to dominate the covariance matrix, given that they are more highly correlated with each other than those around the equator since they cover a smaller spatial area.

Only data for the years which occurred in all datasets was used, to make for a fair comparison. Data for the 20CR and for ERA-40 is grouped into 6-hourly timesteps. There

was some concern that the diurnal cycle may affect the dof calculations and so daily average values were calculated and it was these that were used. The seasonal cycle could also affect the results as this trend would dominate the covariance matrix, leading to one disproportionately high eigenvalue and thus a very small number of dof. To counteract this each calculation is performed twelve times, once for each month. This will also indicate how dof vary from season to season. This has been done to some extent in previous studies, although most research up to this point has simply performed 'summertime' and 'wintertime' calculations, rather than detailed accounts of month-by-month variations.

The HadSLP2 dataset uses monthly-averaged values and so when comparing dof for this with those for the 20CR and ERA-40, monthly averages will be calculated and used for both reanalyses. The reanalysis datasets will also use 1000hPa values since this is the lowest level used in the reanalyses and so will make for the most constructive comparison with SLP. Similarly, geopotential height rather than temperature data will be used for this comparison since it is a more closely related variable.

3.3.3 – Variable Parameters

Several different parameters were chosen to be varied. These were atmospheric variable, temporal resolution, latitude, zone, pressure level and decade. These will be varied and the dof calculated for both the 20CR and ERA-40; the difference between their results will be found and analysed. The considerations specific to each parameter are discussed below.

Atmospheric Variable

Two different variables were chosen to have dof calculated for; these were temperature and geopotential height. These were selected for a number of reasons; firstly because 6-hourly data was available for them for both the 20CR and ERA-40, as it was not for many other variables. Temperature was chosen since it is known to be well represented in ERA-40 (Uppala et al. 2004), and since we are taking ERA-40 as truth for the purposes of this study, accuracy is an important criterion. Geopotential height was selected as it is the primary indicator of atmospheric flow and as such is an excellent gauge for atmospheric complexity.

Temporal Resolution

Dof will be calculated for 6-hourly, daily and monthly data to investigate how it varies with temporal resolution. This will be done by averaging the data over the appropriate time intervals for each gridcell. Comparing the 6-hourly and daily results will indicate if the diurnal cycle does indeed effect the dof calculations. The results will also indicate how much of the complexity in the datasets stems from short-lived phenomena by how much the dof drops when moving to longer timesteps.

Latitude

Dof calculations will be performed for the latitude bands 0°-30°N, 30°-60°N and 60°-90°N (or more precisely -1.25 – 28.75°N, 28.75 – 58.75°N and 58.75 - 88.75°N). These are deemed to be sufficiently large to encompass large weather systems whilst being a convenient division of the tropics, mid-latitudes and high-latitudes. These are performed to investigate how dof vary across latitudes and how well these variations are represented in each reanalysis dataset. The results will be scaled by geographical area using the 30°-60° band as a base unit. Thus the dof that each band would have if they had equal areas can be compared.

Zone

Dofs are calculated for each of five zonal areas. These all cover the area from 30°N to 70°N for the following longitudes:

- European zone: 357.5°E – 65°E
- Asian zone: 70°E – 137.5°E
- Pacific zone: 142.5°E - 210°E
- North American and Canadian zone: 212.5°E - 280°E
- Atlantic zone: 285°E – 352.5°E

These areas all are of equal size so that a fair comparison of the dof between them can be made. The positioning of the zonal regions was chosen to ensure that each continent in the NH had its own zone and that the storm track regions in the Pacific and Atlantic oceans were included; (locations of storm track regions were taken from Swanson & Pierrehumbert (1997)

and Plougenven et al. (2003)). These calculations are performed to investigate how dof vary across zones and how well these variations are represented in each reanalysis dataset.

Pressure Level

Dof calculations will be conducted for several different pressure levels; these are 1000hPa, 850hPa, 700hPa, 500hPa, 250hPa and 100hPa. These were chosen as data is available for them for both reanalysis datasets and because they cover a wide range of values. Previous research (Fraedrich et al. 1995) has suggested that dof increase with height; this will be investigated, along with how well this trend is represented in each reanalysis dataset.

Decade

Dof will also be calculated for each reanalysis dataset on a decade-by-decade basis. Throughout the periods covered by the reanalyses, the number of observations available increased. This study will investigate how such an increase affects the number of dof. This should tell us for what period the 20CR is the most reliable. It was decided to start each decade at the year '$10n + 2$' for a given n, i.e. 1872, 1882, etc.; this maximises the number of decades available for both the 20CR and ERA-40. Decadal dof will be calculated for the whole NH and for the area 30°N and above. This is because Compo et al. (2006) calculated that the quality of the 700hPa geopotential height reanalysed data would not vary over the twentieth century for the NH extra-tropics and this assertion will be tested in this study.

For each of these parameters, suitable graphs will be plotted to compare results from the different datasets. Chequerboard plots will also be created in which colours are assigned to a

grid based on the value of the number of dof in one dataset minus the number of dof in another. These should assist in identifying trends in the results.

3.3.4 – EOF Plots

The Nef formula involves calculating the eigenvalues of the covariance matrix of the gridcell anomalies. The corresponding eigenvectors will give us the component loadings of each principle component. Thus these eigenvectors will be calculated and the loadings from the first six will be plotted onto a NH map so that the dominant trends in the data can be identified. Doing this for both the 20CR and ERA-40 will show whether the same patterns are dominant in each or not.

Results

4.1 – Introduction

This chapter has five main sections, one relating to each of this study's objectives. Section 4.4 (Objective 3) is divided into three sections, one each for the results from varying latitude band, zonal region and pressure level.

4.2 – Objective 1

The first results are how degrees of freedom in the 20CR and ERA-40 vary across the time periods covered by these datasets. These are all calculated for daily data at 500hPa. Decades are numbered from 1 (1872-1881) up to 13 (1992-2001); ERA-40 begins with decade 10 (1962-1971). Results from both the Nef and the Nmm formulae are given for both temperature and geopotential height data. Dof were calculated for the whole NH and for the NH extratropics; first are the 20CR results for the whole NH:

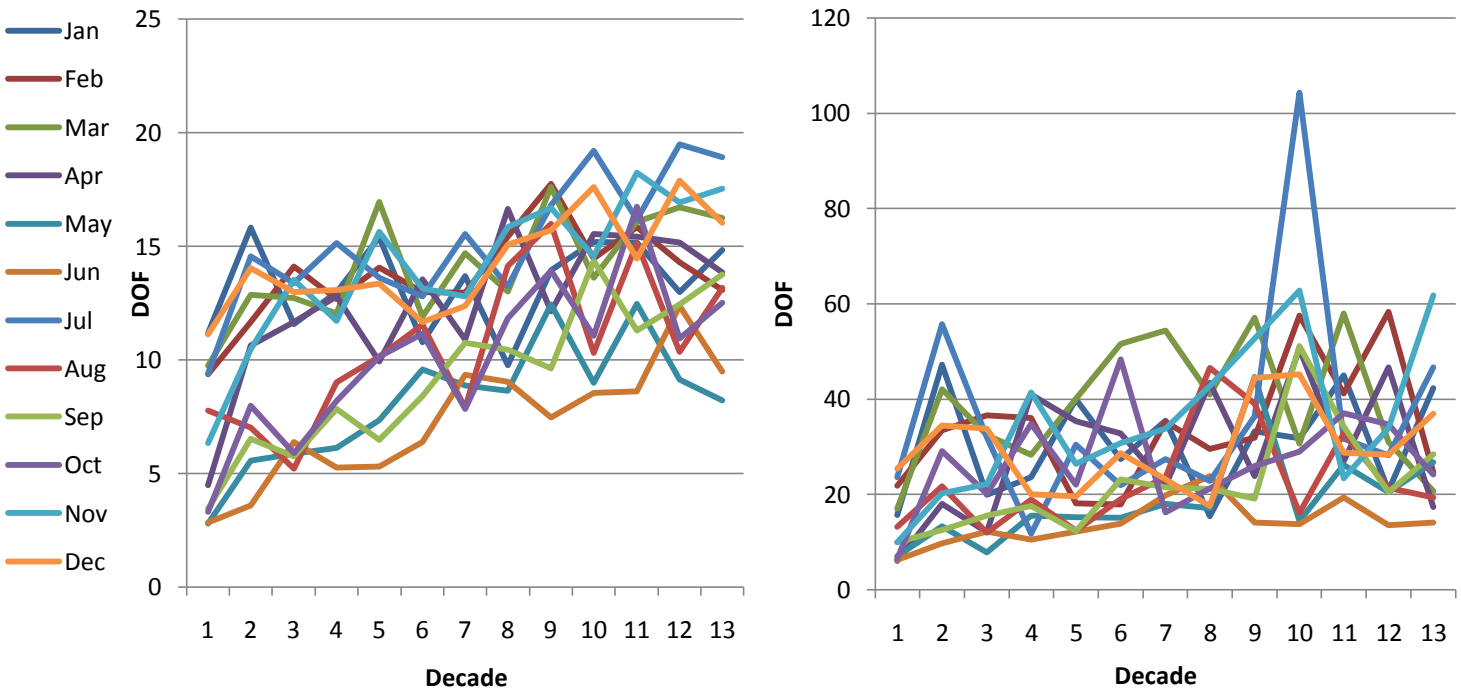

Fig 4.2.1: 20CR dof for 500hPa NH daily temperature data on a decadal basis using the Nef formula (left) and the Nmm formula (right)

Now 20CR results for geopotential height data:

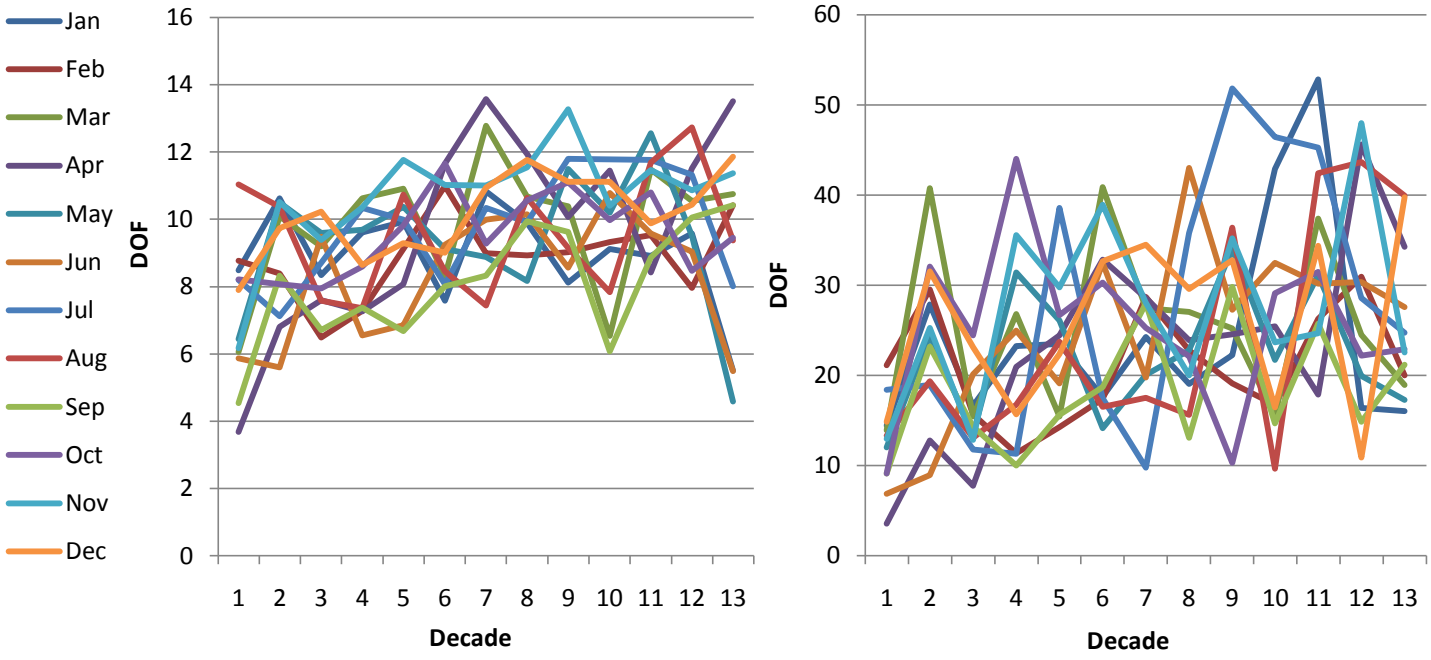

Fig 4.2.2: 20CR dof for 500hPa NH daily geopotential height data on a decadal basis using the Nef formula (left) and the Nmm formula (right)

For both temperature and geopotential height data an increase across the time period can be observed.

Similar graphs can be plotted for ERA-40 dof:

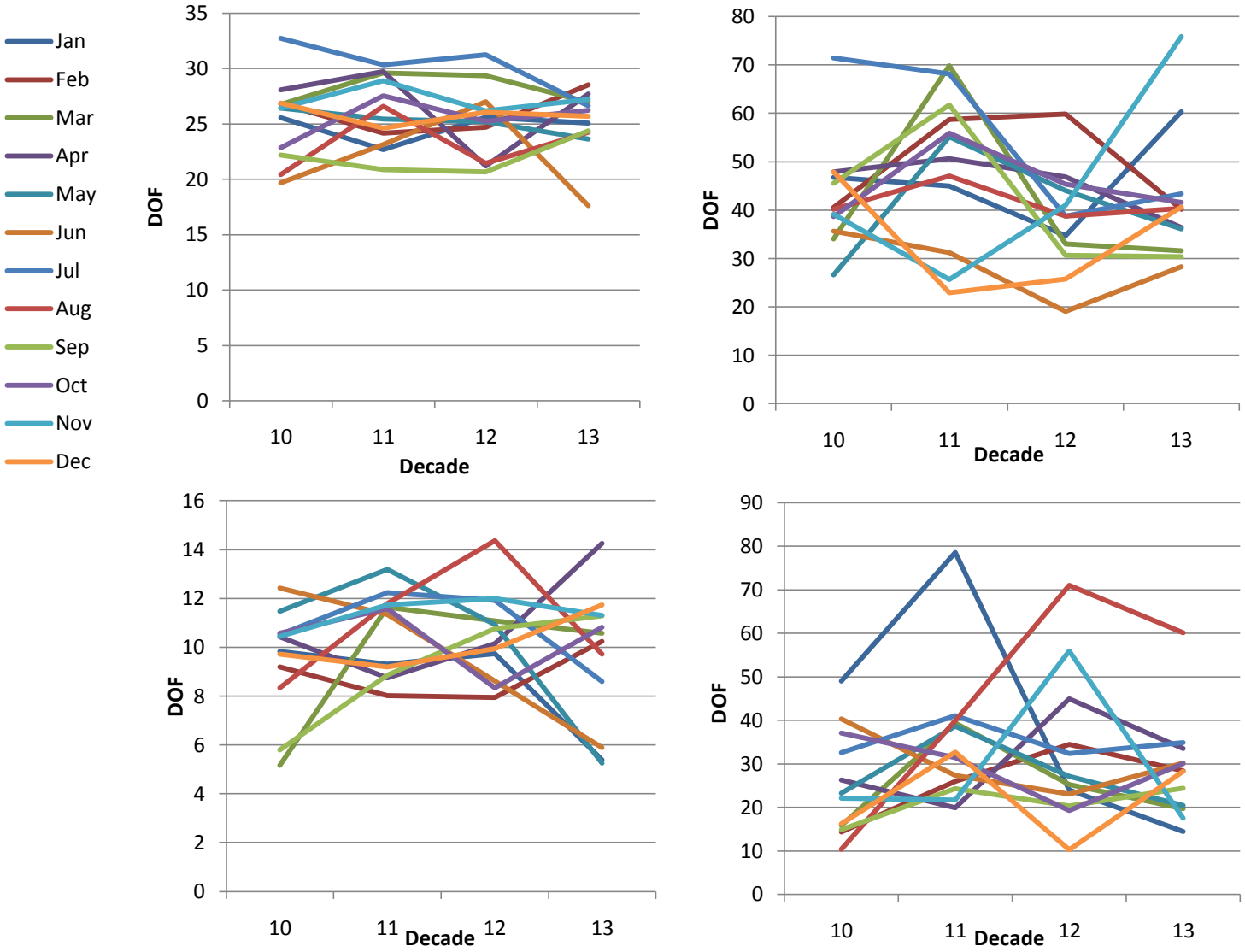

Fig 4.2.3: ERA-40 dof for 500hPa NH daily temperature (above) and geopotential height (below) data on a decadal basis using the Nef formula (left) and the Nmm formula (right)

Here are the equivalent 20CR results for the NH extratropics:

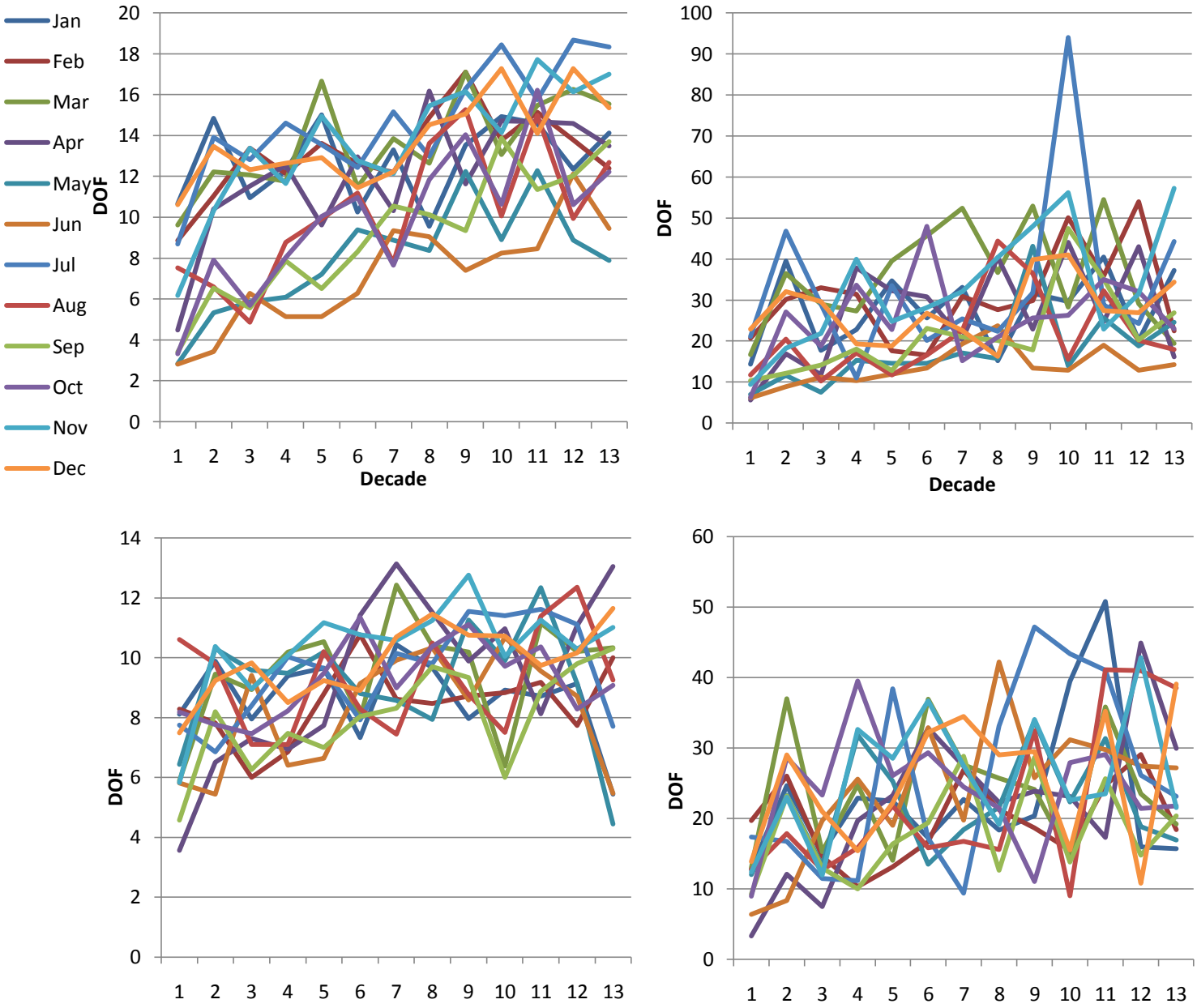

Fig 4.2.4: 20CR dof for 500hPa NH extratropics daily temperature (above) and geopotential height (below) data on a decadal basis using the Nef formula (left) and the Nmm formula (right)

4.3 – Objective 2

Dof have been calculated for both variables at 6-hourly, daily and monthly resolutions for both the 20CR and ERA-40. The results for the temperature data are as follows:

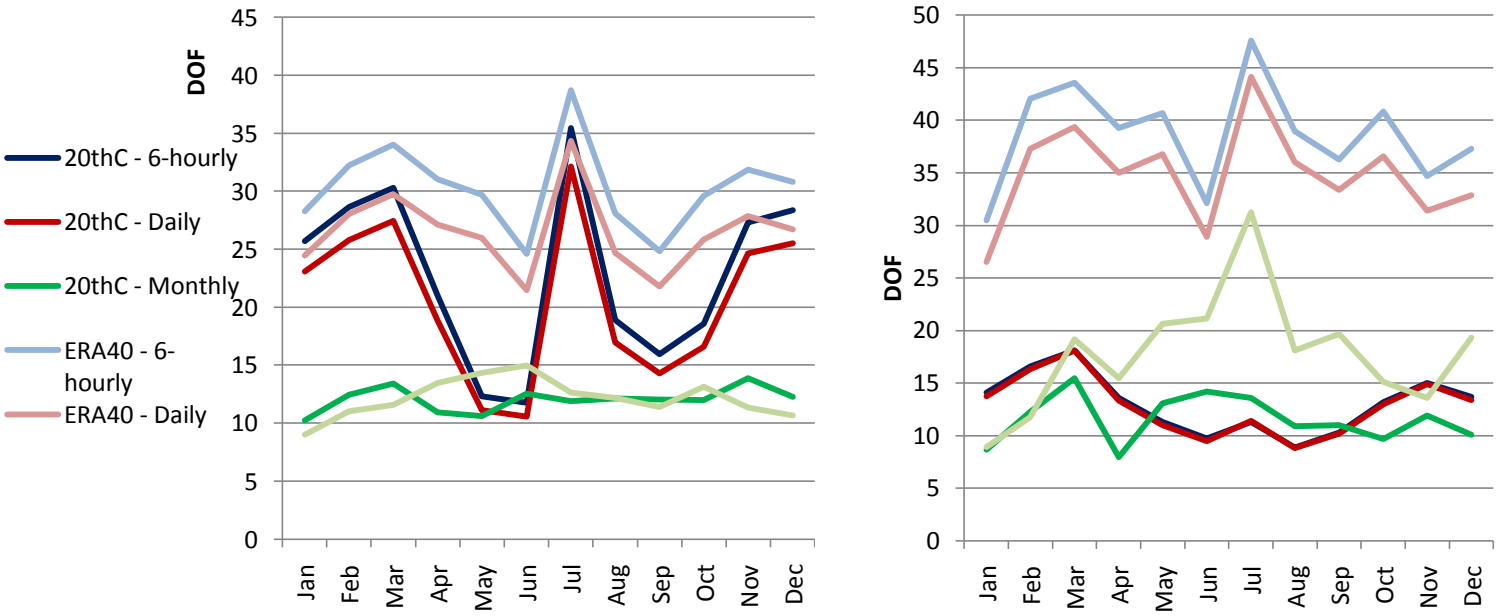

Fig 4.3.1: Dof for the 20CR and ERA-40 at varying temporal resolutions for 500hPa NH temperature data using the Nef formula (left) and the Nmm formula (right)

The Nef formula results show a distinct annual pattern of higher numbers of dof in summer and winter and lower values in spring and autumn. The number of dof in the ERA-40 data is consistently above that in the 20CR data, though for the Nef formula they do follow a similar annual cycle. The dof in the daily data are slightly less than those in the 6-hourly data though they do follow the same annual pattern. There are considerably fewer dof in the monthly data than the 6-hourly or daily data. For the Nmm results the 20CR dof are similar at all temporal resolutions. In contrast, the ERA-40 results have a wide spread between the different temporal resolutions.

Here are the equivalent plots for geopotential height:

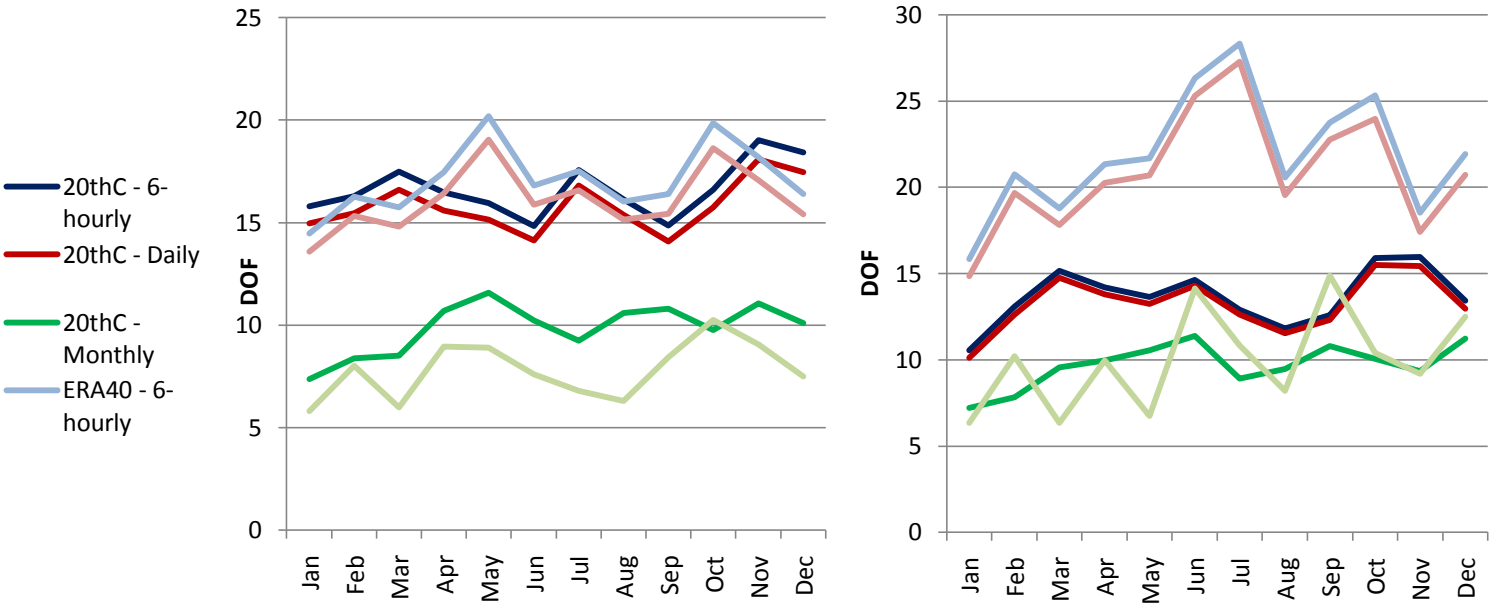

Fig 4.3.2: Dof for the 20CR and ERA-40 at varying temporal resolutions for 500hPa NH geopotential height data using the Nef formula (left) and the Nmm formula (right)

These show far less variation in the number of dof over the course of a year, and while for the Nef results the 20CR dof show a similar pattern to those for temperature, for ERA-40 the annual cycle is completely different.

The difference between the ERA-40 and 20CR dof at different temporal resolutions can be shown by the following chequerboard plots:

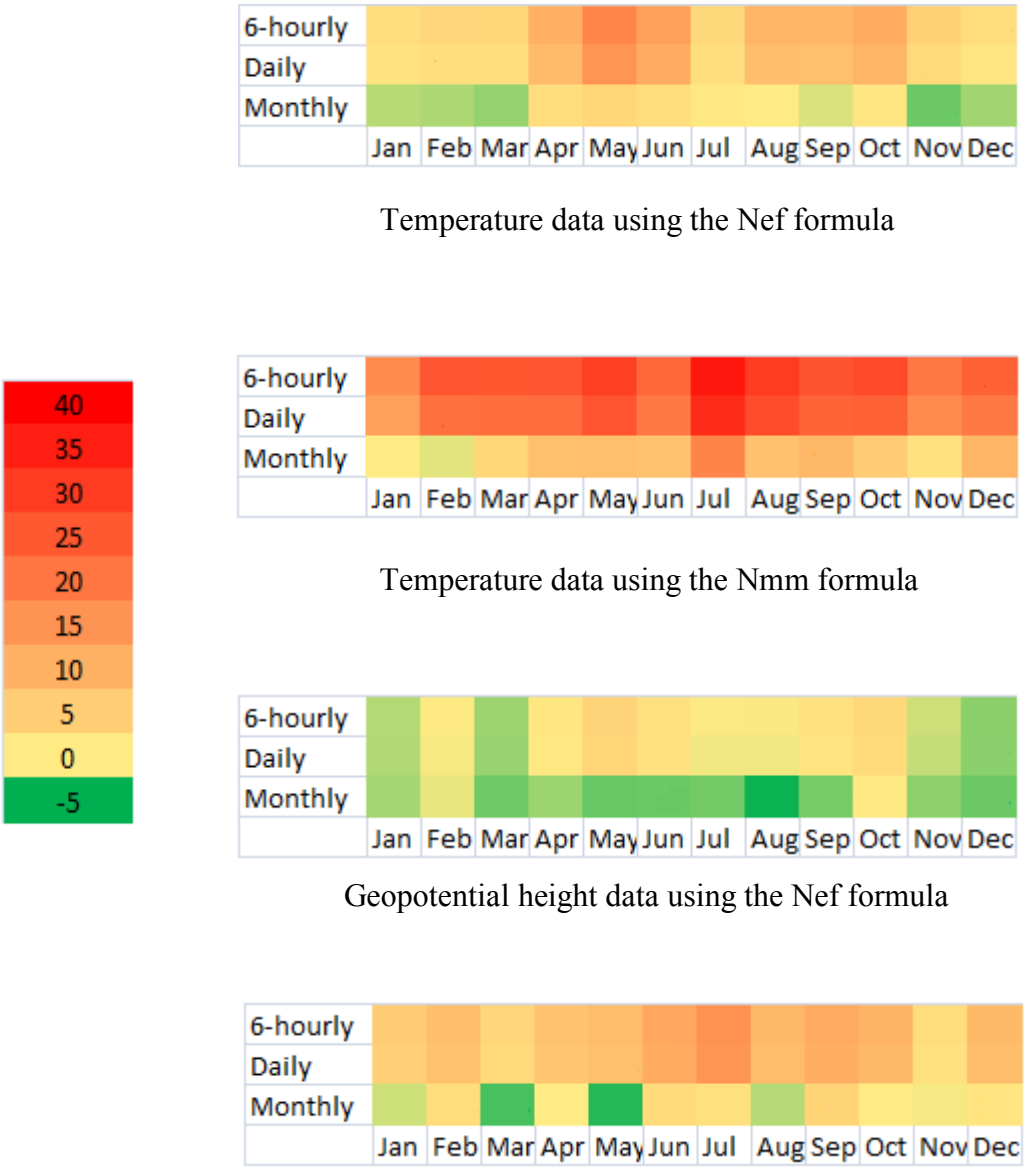

Fig 4.3.3: Chequerboard plots of ERA-40 dof minus 20CR dof for 500hPa NH data at varying temporal resolutions

These show that ERA-40 dof exceed 20CR dof by the greatest margin in summertime at the higher temporal resolutions. The Nmm formula tends to produce a larger difference between

the 20CR and ERA-40 dof than the Nef formula and the two datasets tend to be in closer agreement regarding geopotential height data rather than temperature data.

4.4 – Objective 3

4.4.1 – Latitude Bands

Dof have been calculated for each reanalysis dataset for each variable at 3 different latitude bands. These use daily mean data at the 500hPa level and the results have been scaled so that they all represent the dof that would exist over an area equal to that of the 30 - 60°N band. The results for the temperature data are as follows:

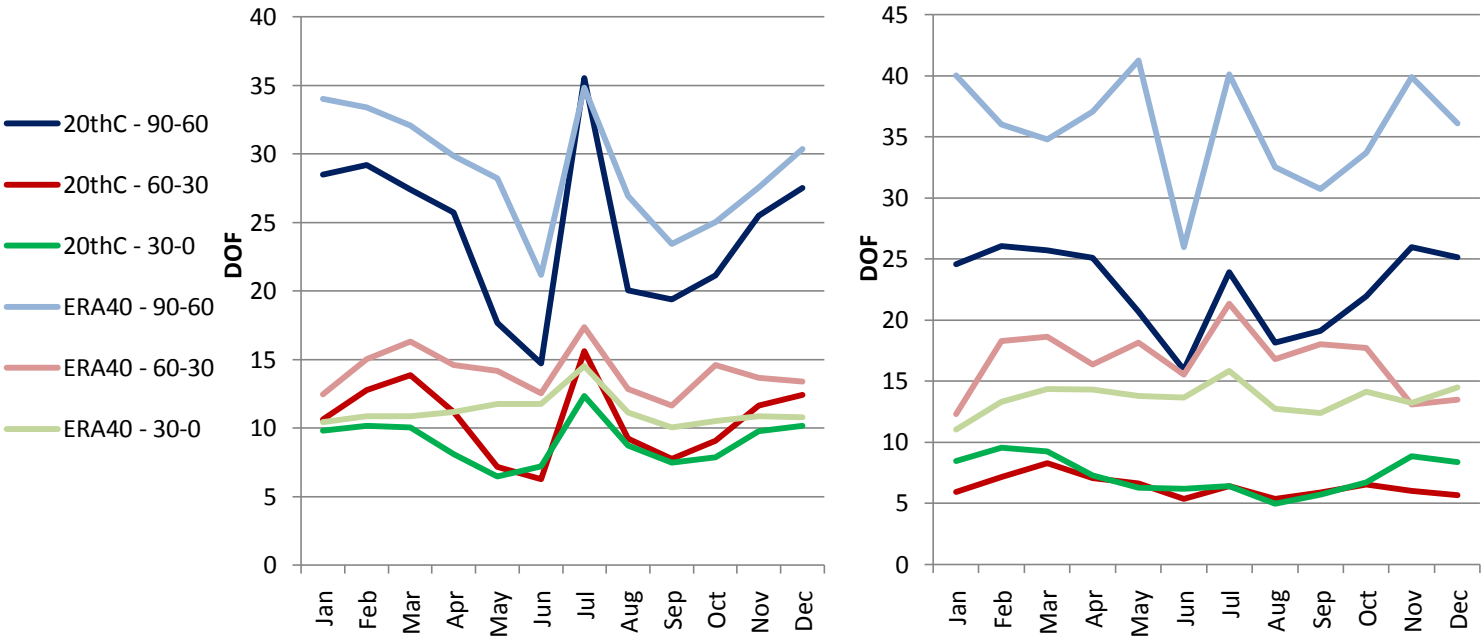

Fig 4.4.1.1: Dof for the 20CR and ERA-40 for different latitude bands for 500hPa NH daily temperature data using the Nef formula (left) and the Nmm formula (right)

For the Nef results, the same annual cycle as could be seen in the equivalent plot for varying temporal resolutions, with high values in summer and winter and lower values in spring and autumn, is apparent. There are significantly more dof at high latitudes than in other areas and the mid-latitudes and tropics have similar numbers of dof.

Here are the geopotential height results:

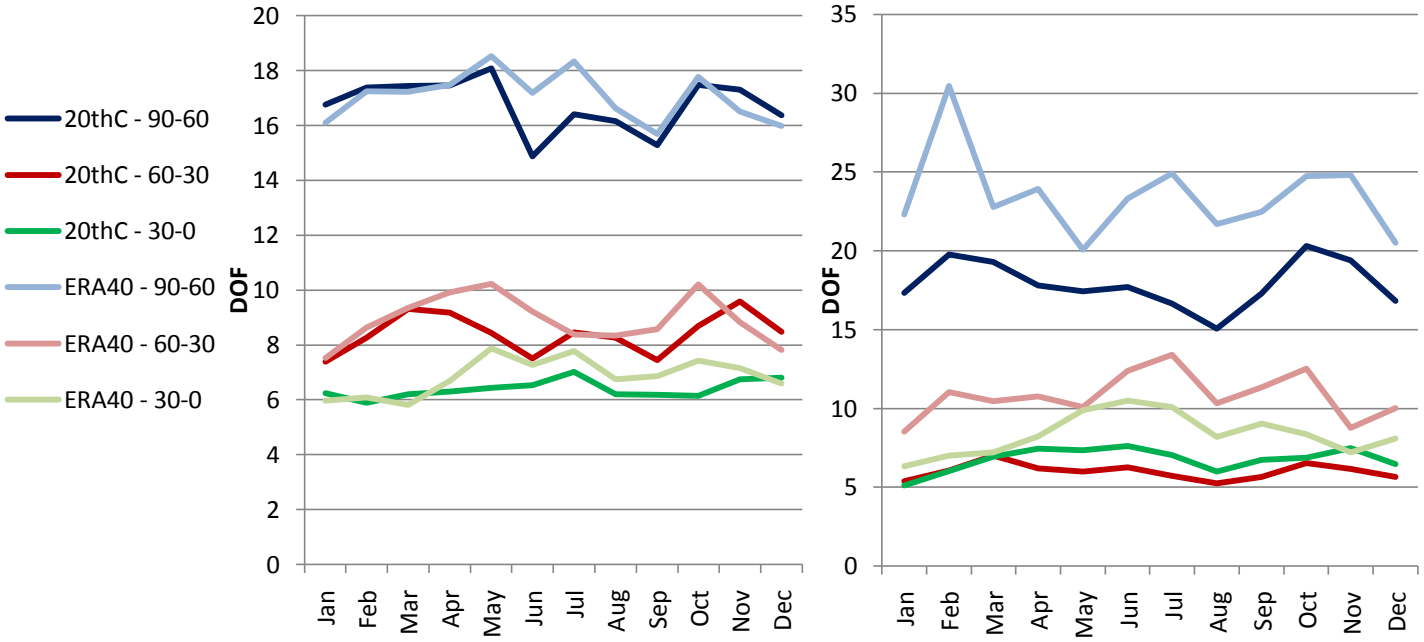

Fig 4.4.1.2: Dof for the 20CR and ERA-40 for different latitude bands for 500hPa NH daily geopotential height data using the Nef formula (left) and the Nmm formula (right)

These show substantially less annual variation than the equivalent temperature plots, though there are still more dof at high latitudes than in the mid-latitudes or tropics, which remain very similar.

Chequerboard plots can be made to show the difference between the numbers of dof in the two reanalyses:

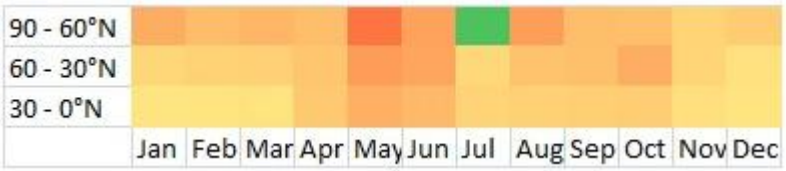

Temperature data using the Nef formula

Temperature data using the Nmm formula

Geopotential height data using the Nef formula

Geopotential height data using the Nmm formula

Fig 4.4.1.3: Chequerboard plots of ERA-40 dof minus 20CR dof for 500hPa NH daily data at different latitude bands

These show that dof in the ERA-40 data exceed those in the 20CR by the greatest amount in the summer months. Also that the two datasets are in closer agreement when considering geopotential height data than temperature data and that the Nef formula tends to produce closer results between the reanalyses than the Nmm formula.

4.4.2 – Zonal Regions

Dof have been calculated for both variables at each of five zonal regions using daily mean data at the 500hPa level. Results for the temperature data are as follows:

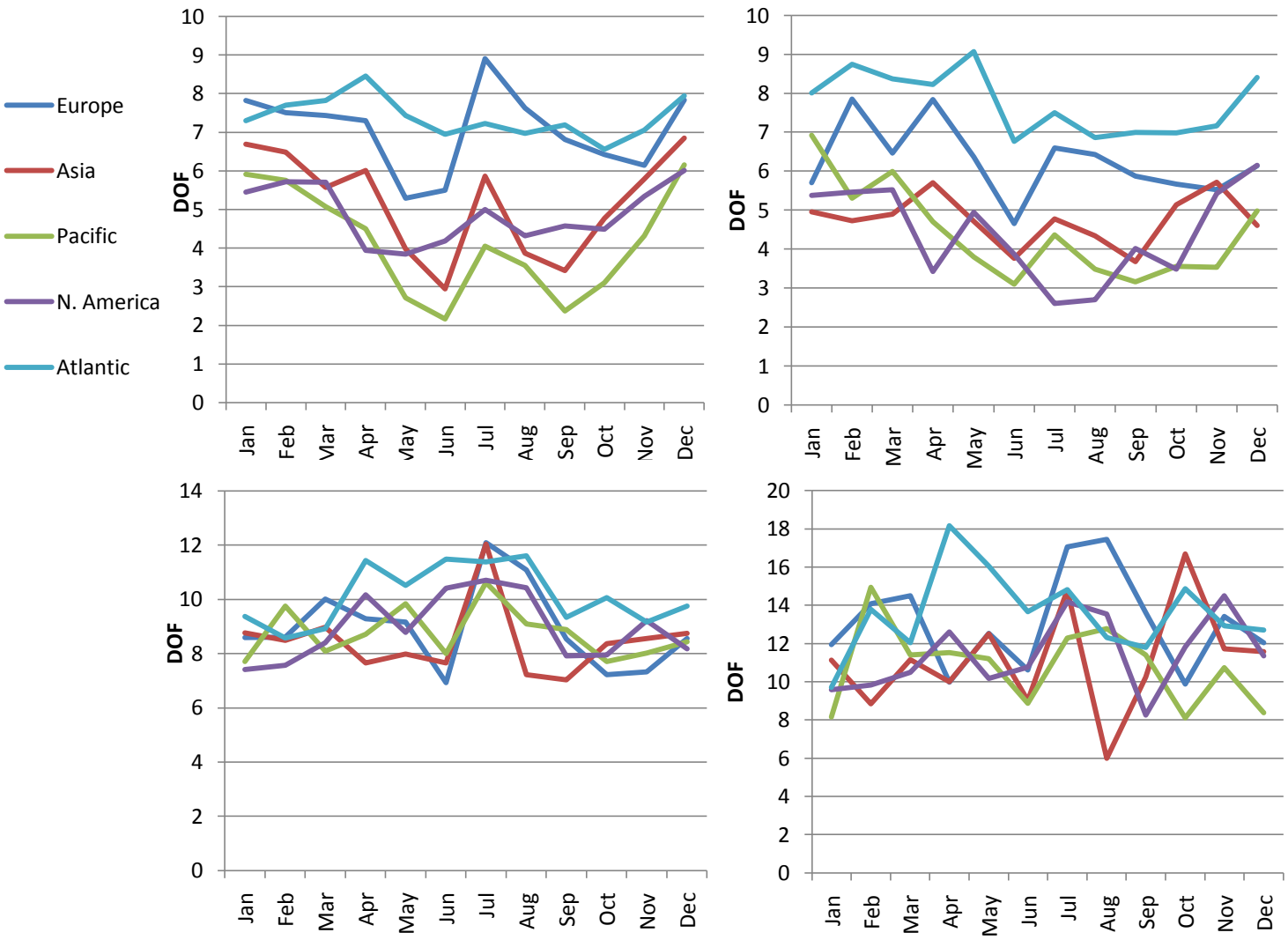

Fig 4.4.2.1: 20CR (above) and ERA-40 (below) dof for 500hPa NH daily temperature data for different zonal regions using the Nef formula (left) and the Nmm formula (right)

There is more variation between the dof for different zones in the 20CR results than for ERA-40. For the results from the geopotential height data, the difference between the dof for different zones is not nearly as pronounced:

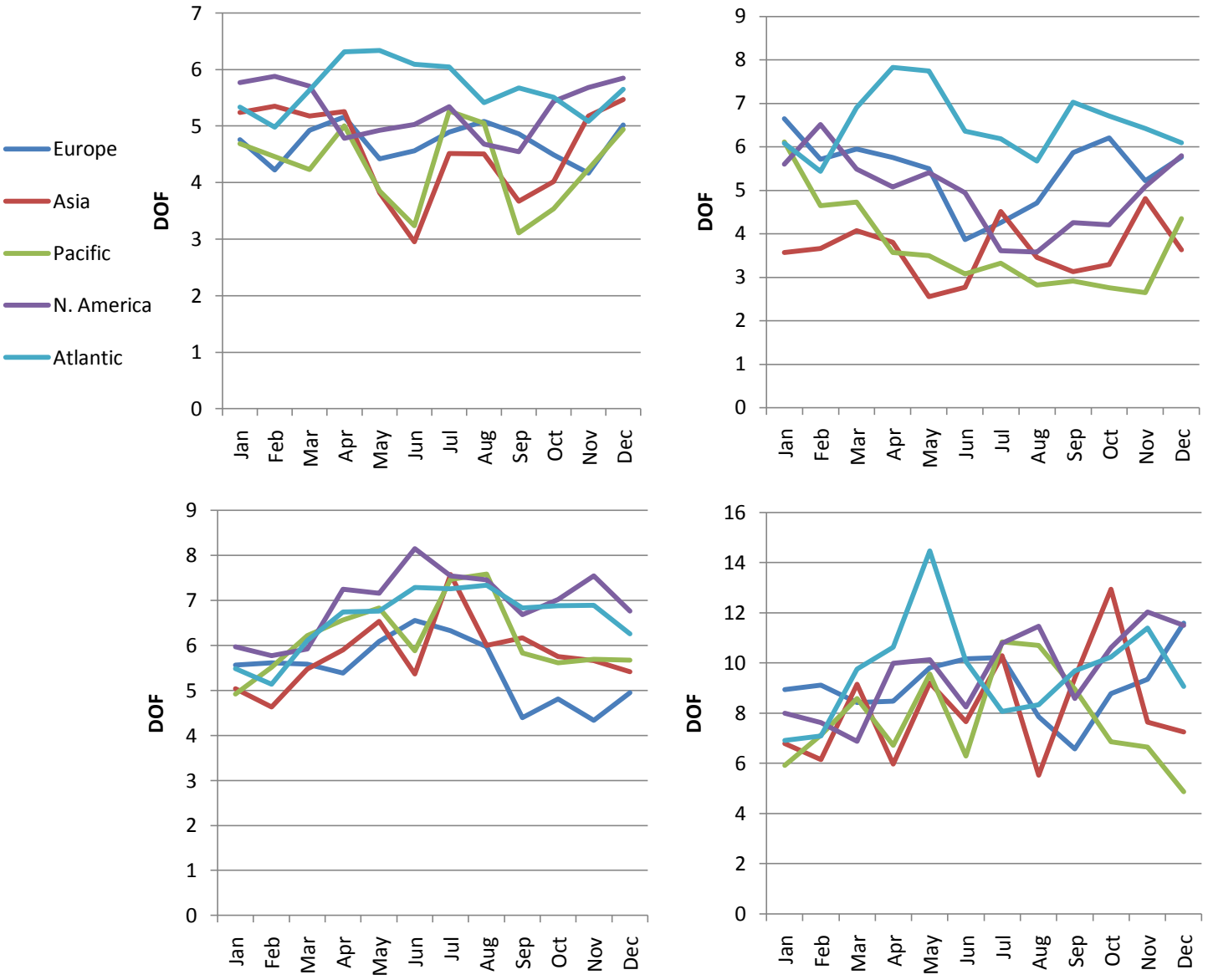

Fig 4.4.2.2: 20CR (above) and ERA-40 (below) dof for 500hPa NH daily geopotential height data for different zonal regions using the Nef formula (left) and the Nmm formula (right)

Here are chequerboard plots for this data:

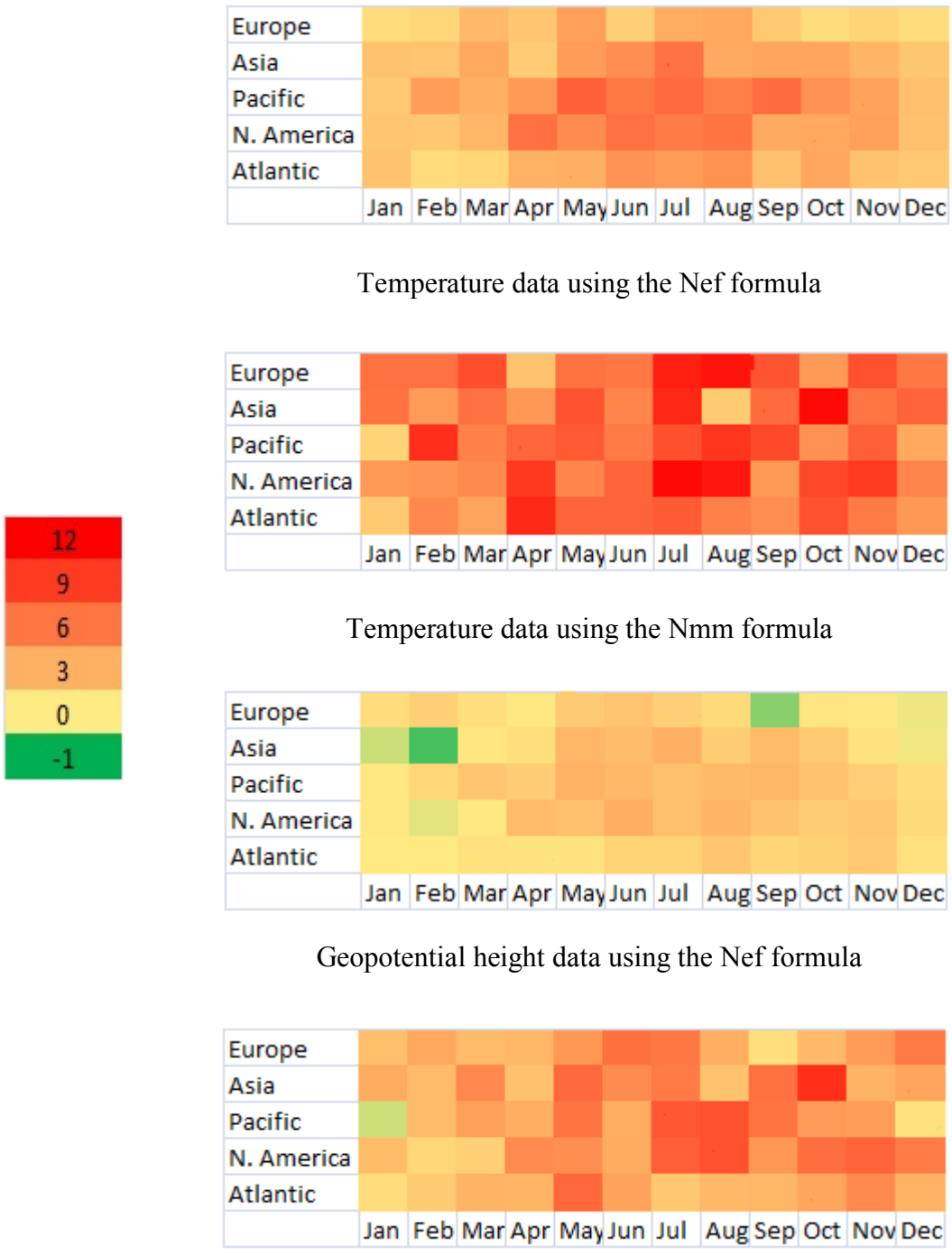

Fig 4.4.2.3: Chequerboard plots of ERA-40 dof minus 20CR dof for 500hPa NH daily data for different zonal regions

The chequerboards for Nef results show that ERA-40 dof exceed those in the 20CR by the greatest margin in summertime in the Asian, northern Pacific and North American regions.

4.4.3 - Pressure Levels

Dof were calculated on each of six pressure levels for both variables; this was done using daily mean data. The results for the temperature data are as follows:

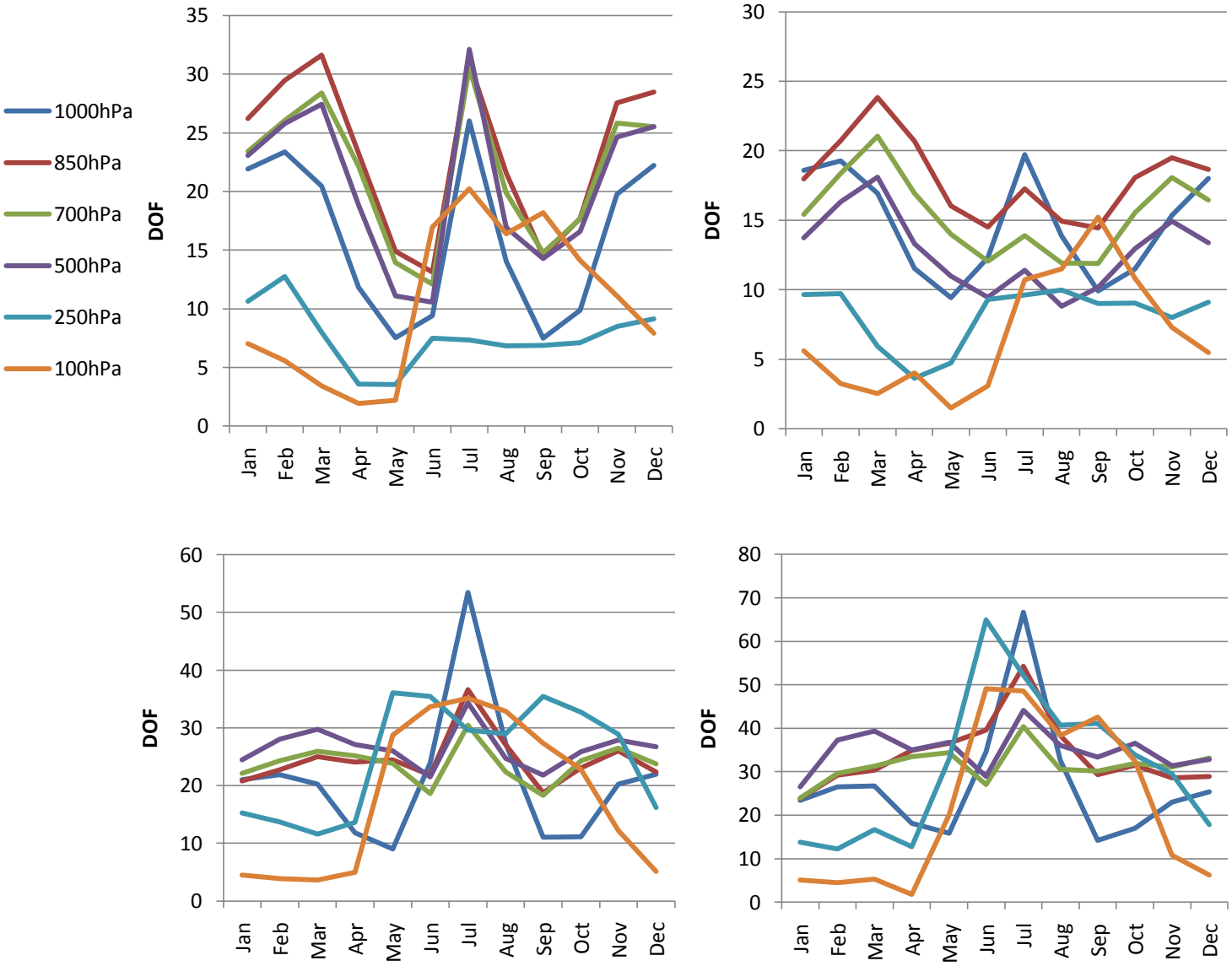

Fig 4.4.3.1: 20CR (above) and ERA-40 (below) dof for NH daily temperature data on different pressure levels using the Nef formula (left) and the Nmm formula (right)

These show that the annual pattern of a peak in July, high values in winter and low values in spring and autumn applies to the lower pressure levels up to and including 500hPa, but above

this it is not so clear, for the most part showing high values in summer and low in winter. The equivalent plots for the geopotential height data are quite different:

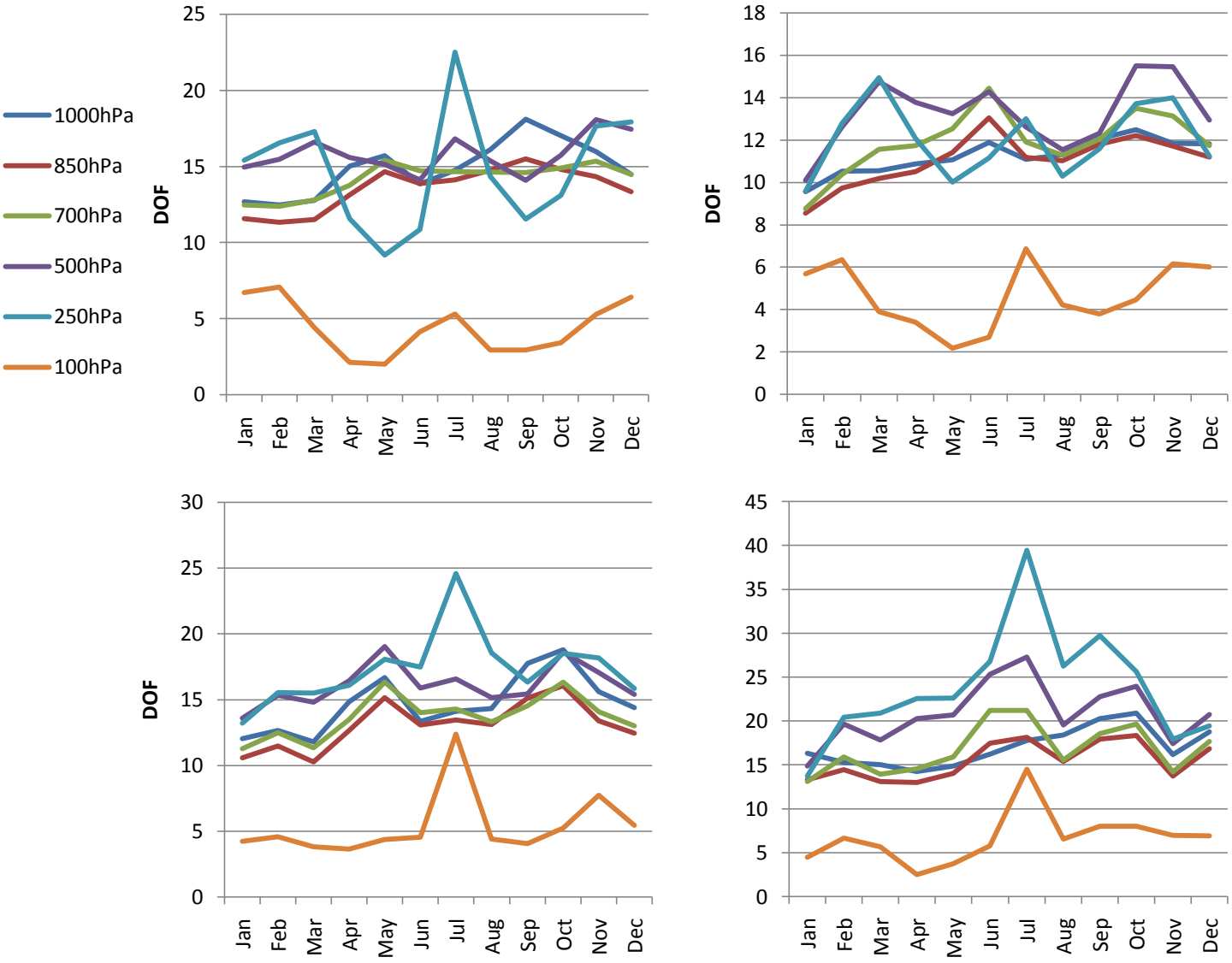

Fig 4.4.3.2: 20CR (above) and ERA-40 (below) dof for NH daily geopotential height data on different pressure levels using the Nef formula (left) and the Nmm formula (right)

These show the upper levels having greater annual variation than the lower ones, with the highest level having noticeably fewer dof than the others.

Here are chequerboard plots for these results:

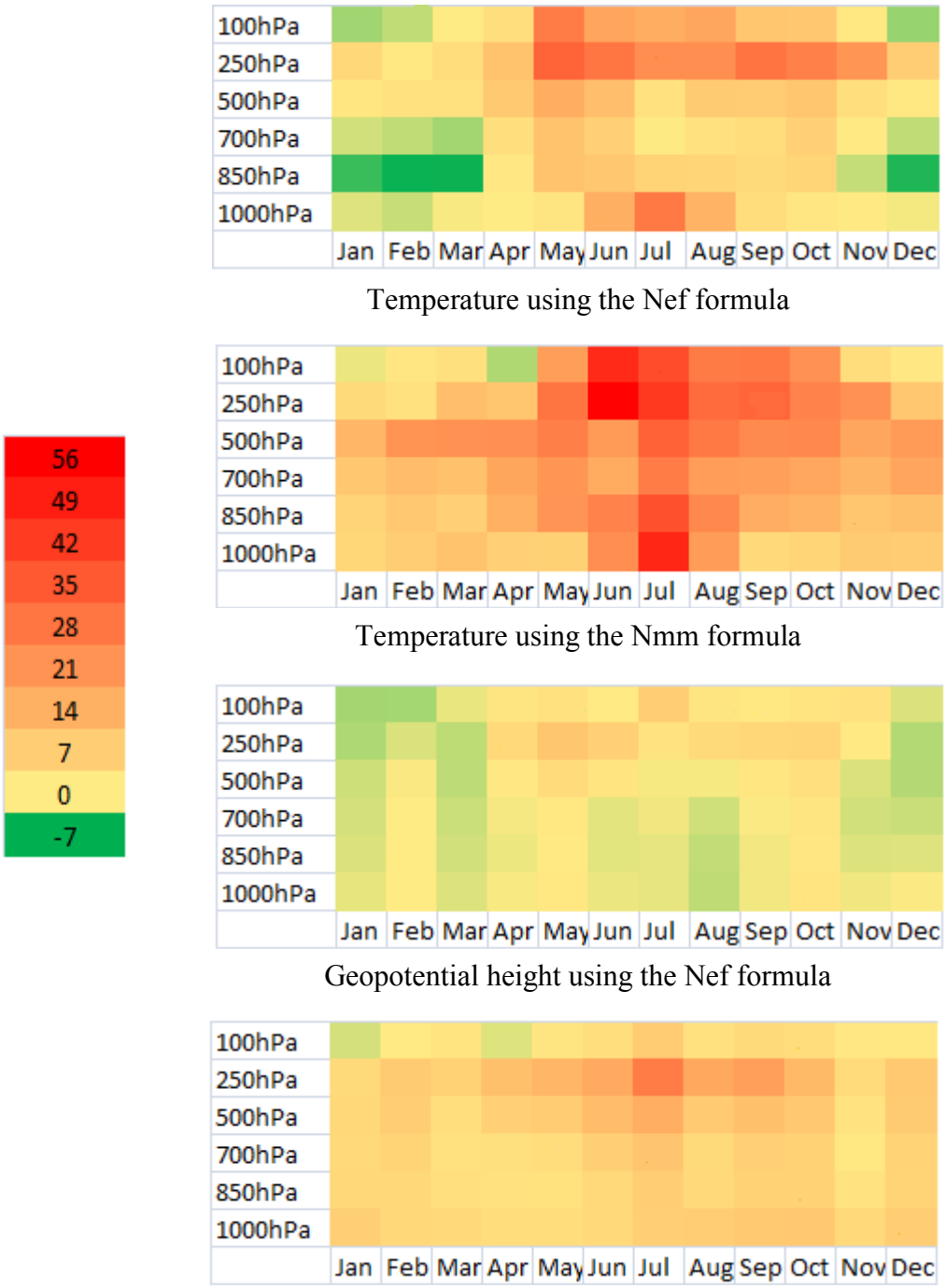

Fig 4.4.3.3: Chequerboard plots of ERA-40 dof minus 20CR dof for NH daily data on different pressure levels

For geopotential height, the margin by which ERA-40 dof exceed those of the 20CR increases with height. There is considerably less difference between ERA-40 and 20CR dof

for geopotential height than for temperature, with those for the 20CR regularly exceeding those for ERA-40 in the Nef plot.

4.5 – Objective 4

Dof were calculated for geopotential height at 1000hPa for both reanalyses and for the HadSLP2 dataset using monthly-averaged data on a 5-degree lat-lon grid. The results are as follows:

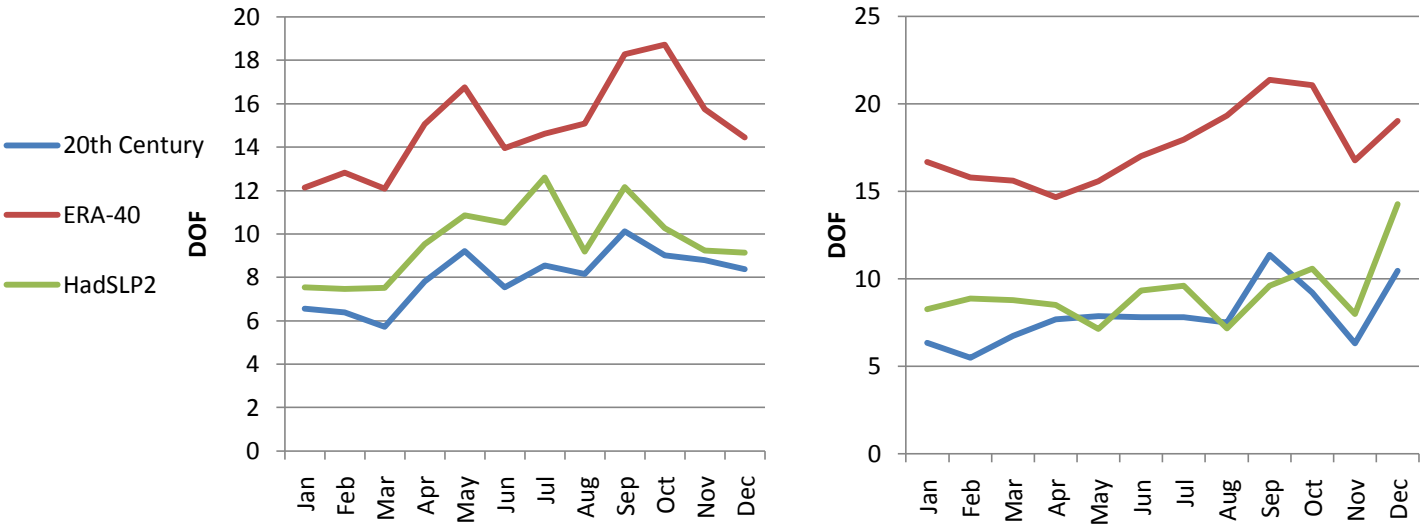

Fig 4.5.1: 20CR, ERA-40 and HadSLP2 dof for NH monthly geopotential height data, at 1000hPa for the reanalysis datasets

The ERA-40 data has the most dof, with the 20CR and HadSLP2 having a similar amount. They all follow approximately the same seasonal cycle, with low values in winter, increasing numbers of dof from March through to May and a high value in September (from Nef plot).

4.6 – Objective 5

The first six leading EOFs were plotted for each variable for both the 20CR and ERA-40 using data at 500hPa with a daily resolution for the months January and July. These are shown on the following pages:

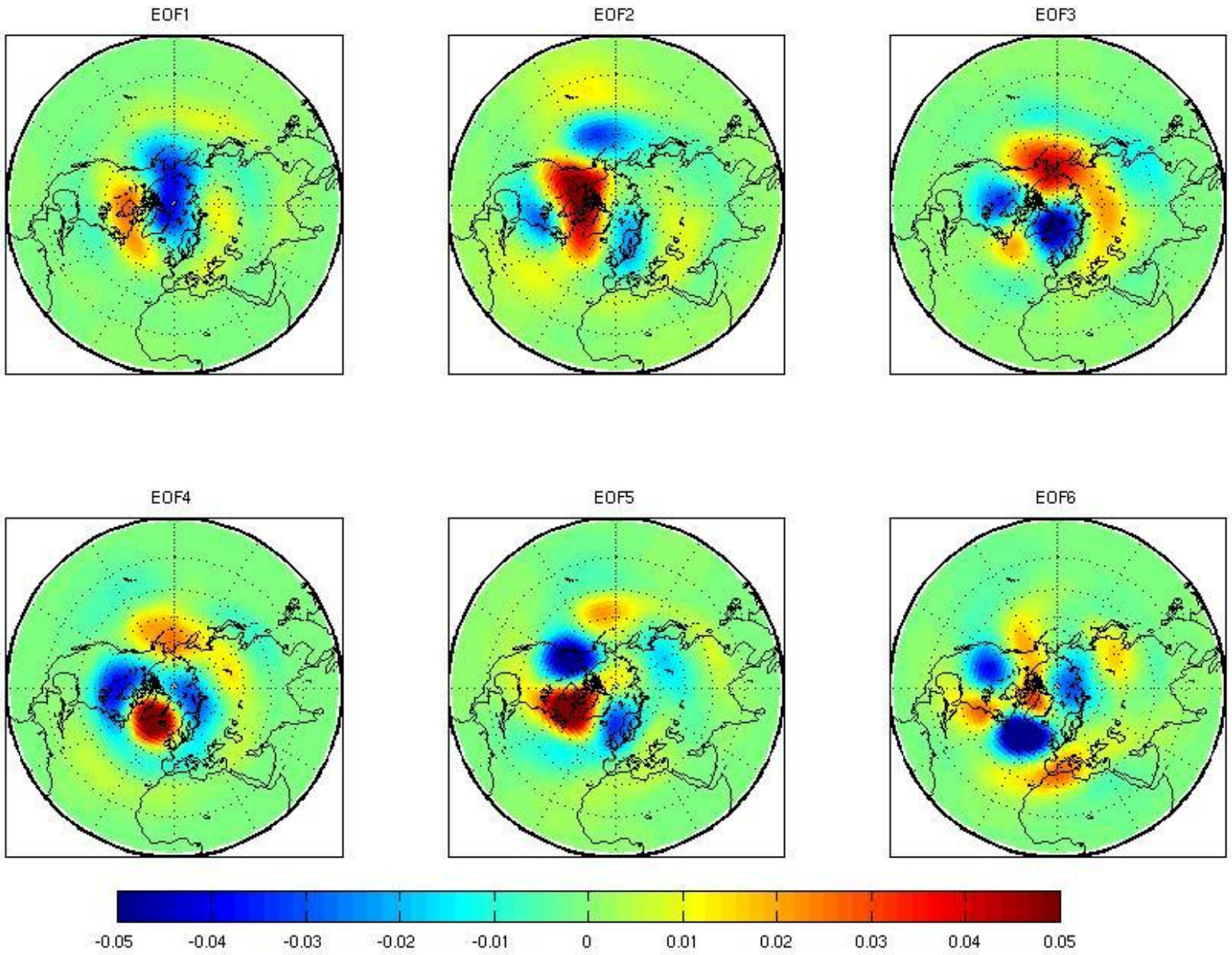

Fig 4.6.1: 20th Century reanalysis first 6 EOFs for January temperature data

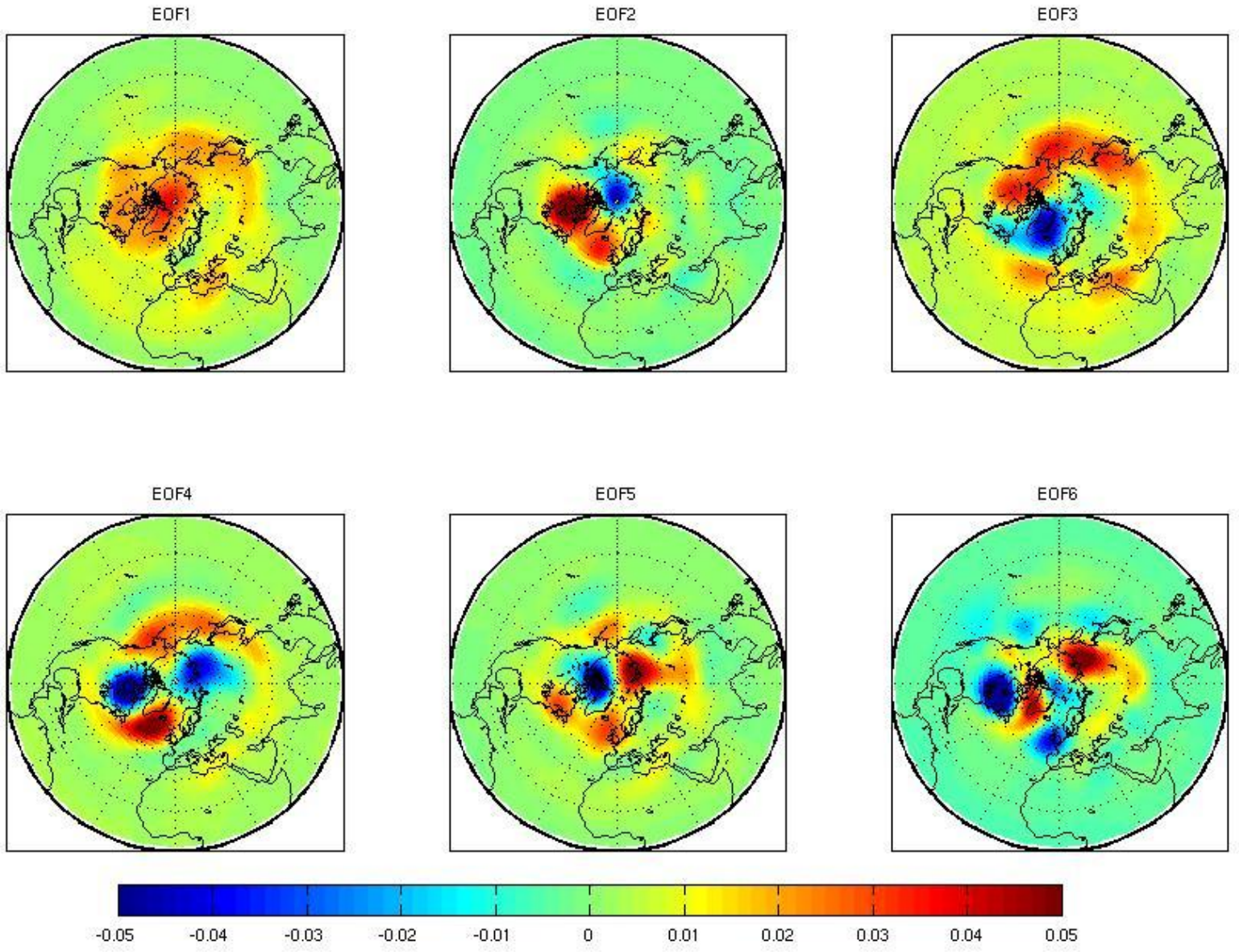

Fig 4.6.2: 20th Century reanalysis first 6 EOFs for July temperature data

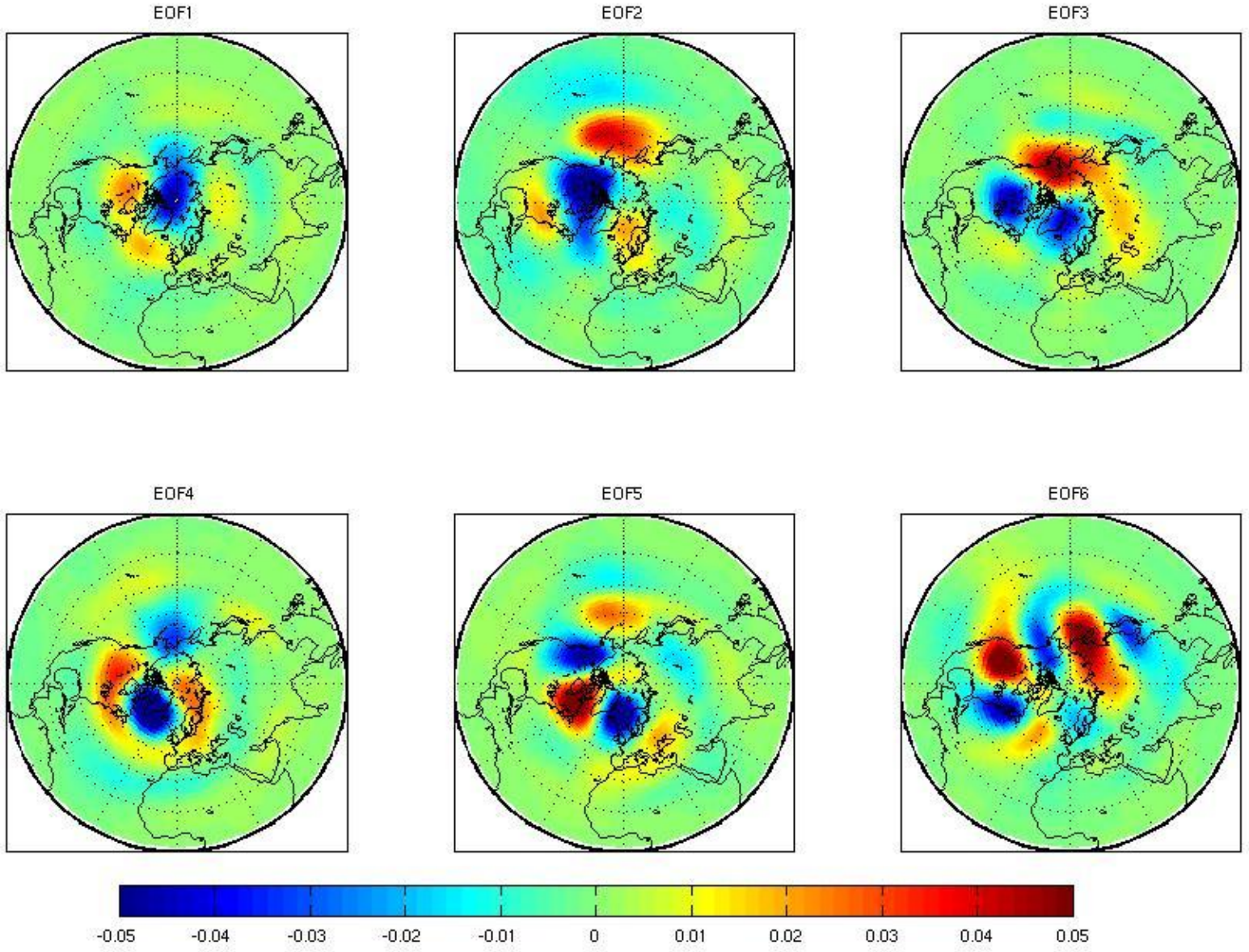

Fig 4.6.3: ERA-40 first 6 EOFs for January temperature data

[72]

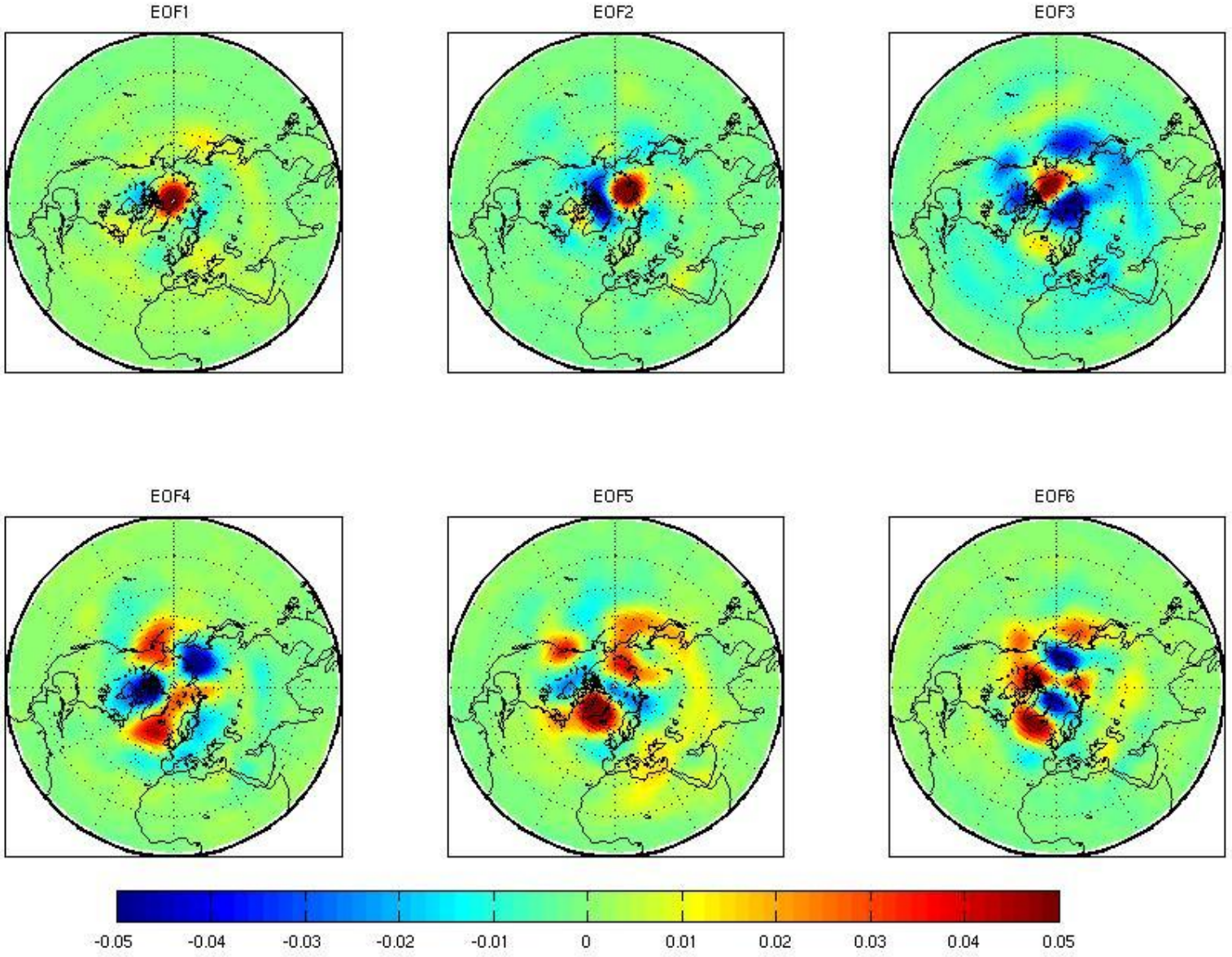

Fig 4.6.4: ERA-40 first 6 EOFs for July temperature data

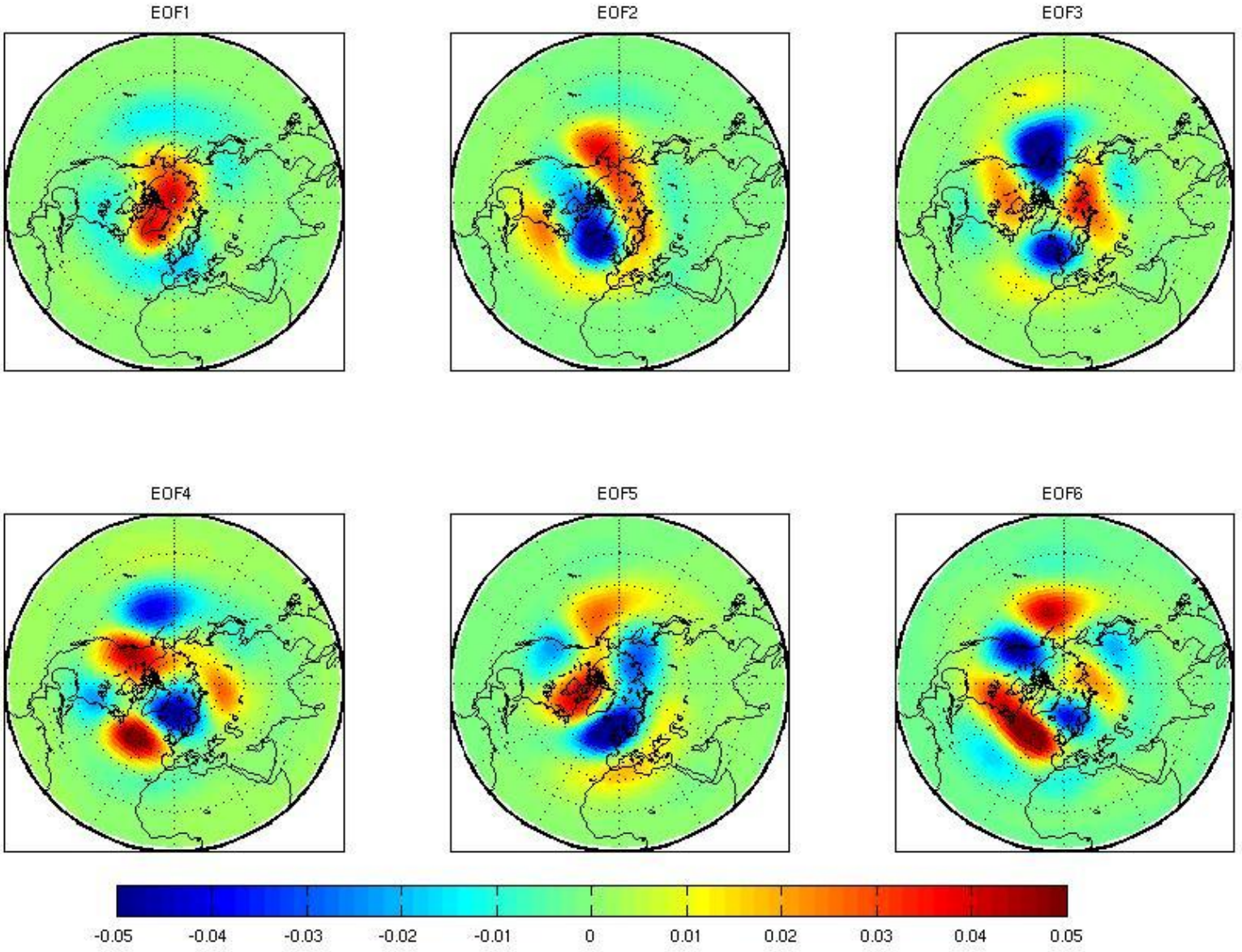

Fig 4.6.5: 20th Century reanalysis first 6 EOFs for January geopotential height data

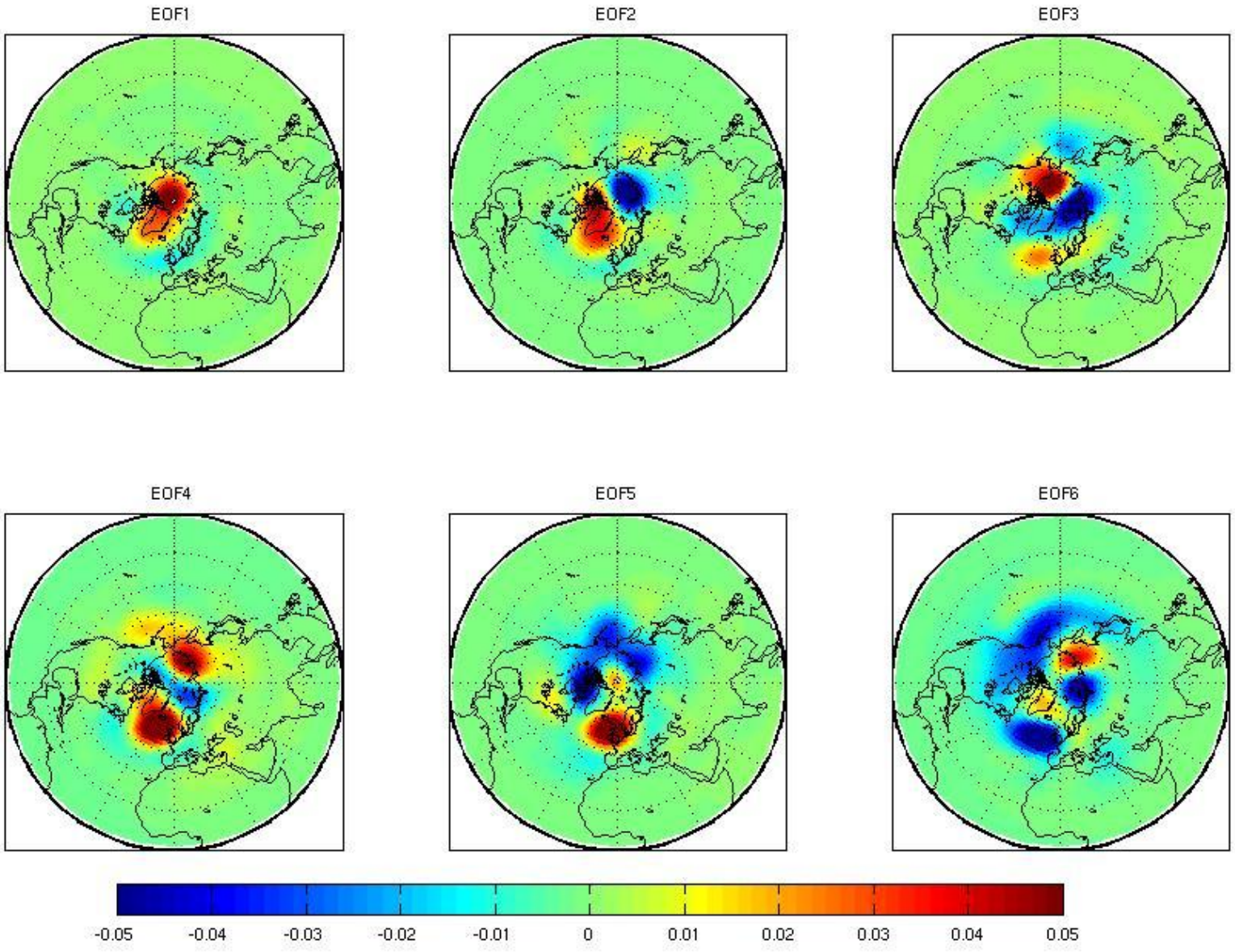

Fig 4.6.5: 20th Century reanalysis first 6 EOFs for July geopotential height data

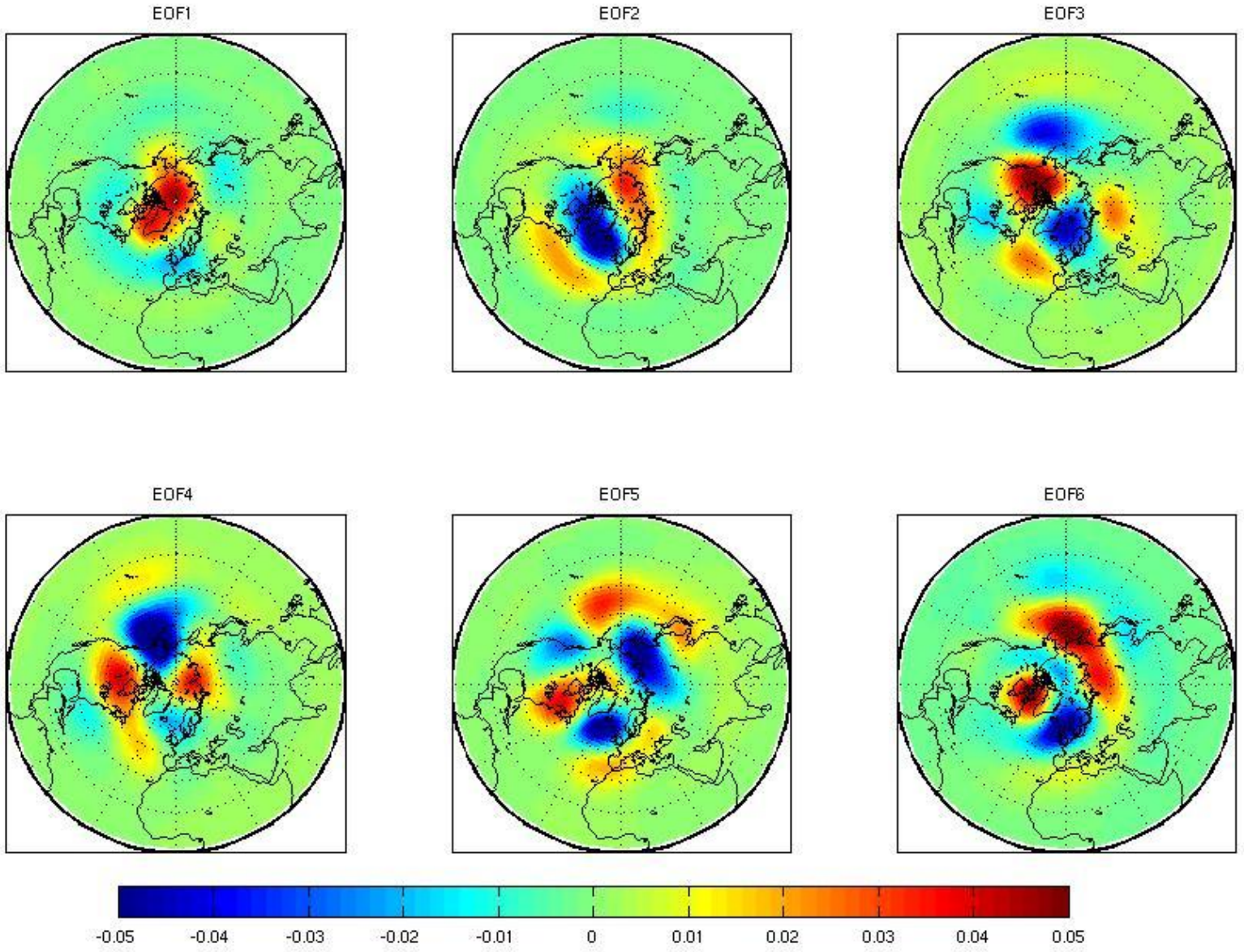

Fig 4.6.7: ERA-40 first 6 EOFs for January geopotential height data

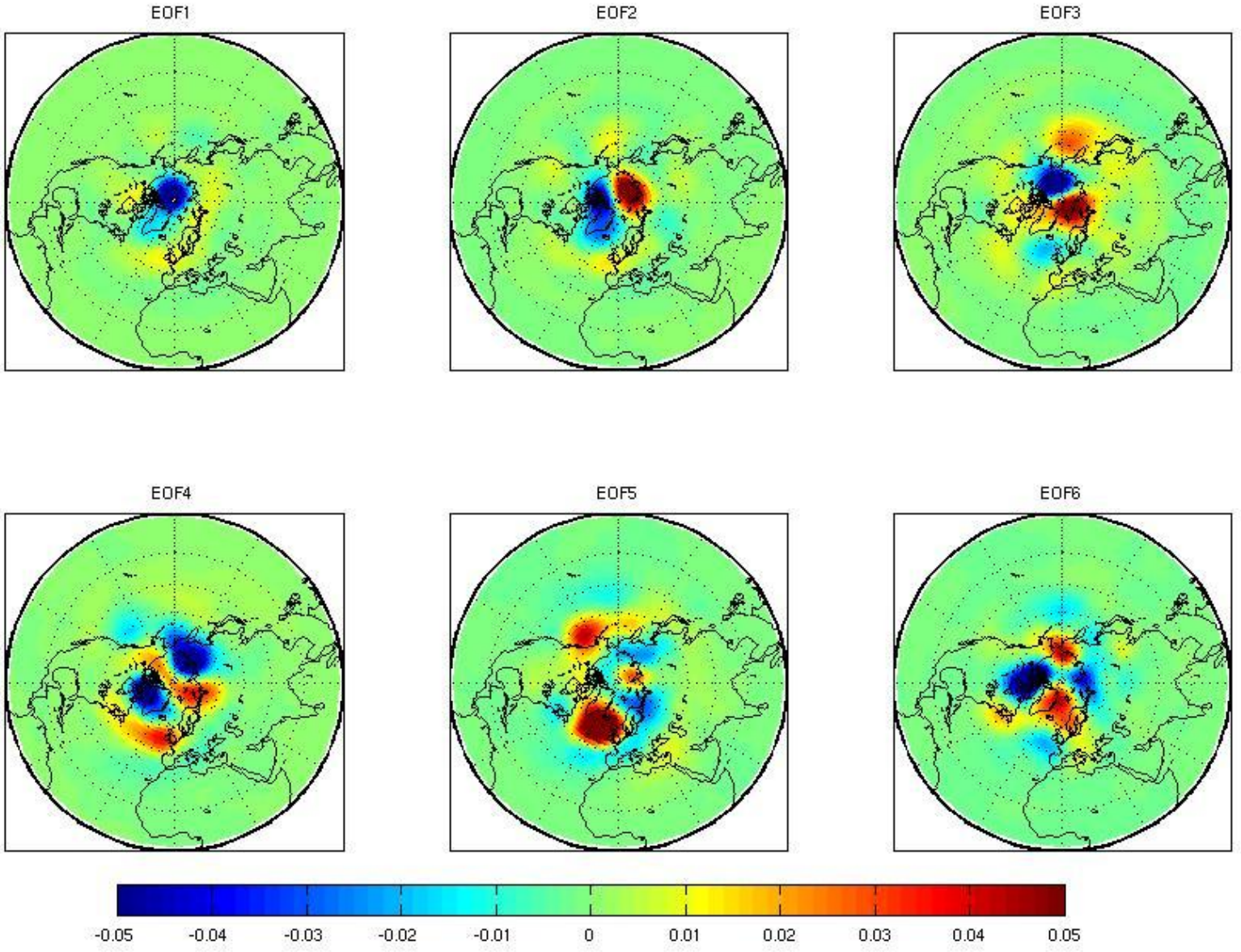

Fig 4.6.8: ERA-40 first 6 EOFs for July geopotential height data

Discussion

5.1 – Introduction

This chapter has 6 main sections; the first is a note on how the results from the Nef and Nmm formulae should be treated; the remaining sections relate to each of this study's objectives in turn. Section 5.5 (Objective 3) is divided into three parts, one each for discussion of the latitude band, zonal region and pressure level results.

5.2 – A Note on the Nef and Nmm formulae

In Bretherton et al.'s study (1999) it was found that for sufficiently short time-series the Nef formula tended to produce results with a small amount of scatter but a relatively large bias. In contrast, the Nmm formula produced results with a low bias but a relatively large amount of scatter. As such, in this study when considering the shape of dof curves, the Nef results will be prioritised as they contain less noise. If there is a large difference in the numbers of dof produced by the two methods then an approximate value will be deduced from the Nmm results.

5.3 – Objective 1

The first thing to note in the decadal dof is the relatively large difference in the outputs from the Nef and Nmm formulae. Thus it is the case that the time-series is short enough to significantly affect the dof estimates. This means that the Nef formula results will be used to deduce trends in the data whilst the Nmm formula results will be used to estimate the numbers of dof. This tells us that the dof increase over the period covered by the 20CR from ~20 to ~35 for 500hPa temperature and from ~15 to ~25 for 500hPa geopotential height.

Compo et al. (2006) calculated that the quality of a reanalysis based on an EnSRF using only surface pressure observations would be consistent throughout the 20th Century for the region north of the tropics for 700hPa geopotential height. They also found that it would increase for the tropics and the SH. If this is the case, then the dof increase calculated in this study is due entirely to increasing numbers of observations in the tropical regions. This can be verified by considering the plots for decade-by-decade dof for the NH extratropics (fig 4.2.4). These are very similar to the equivalent plots for the whole NH and the increasing trend is still clearly visible for both temperature and geopotential height. In their study Compo et al. compared results from 1905 and 1935. Perhaps if they had compared these with those for later years then a difference would have been apparent. Alternatively, in their study they measured reanalysis quality using local anomaly correlation and it may be that a change is less perceptible with this method than with dof. The fact that there was so little difference between these results and those for the whole NH matches what was found when comparing dof for different latitude bands. The band with the smallest number of dof was that covering the tropical region.

For ERA-40 there is no noticeable trend in the results, although with only four values for each month it is difficult to be sure. Uppala et al. (2004) did find that the quality of the 500hPa temperature data in the reanalysis was fairly constant throughout the period and this consistency could be represented in the calculated dof. Calculating dof for shorter time periods (e.g. five years) could make trends easier to detect, although this would likely cause additional bias and spread in the Nef and Nmm formulae respectively making the results increasingly unreliable.

5.4 – Objective 2

The previous dof studies described in section 2.4 in general found that there were more dof in summer than in winter (Livezey & Chen 1983, Van Den Dool & Chervin 1986, Fraedrich et al. 1995, Wang & Shen 1999). For the Nef formula this is technically true although the difference between summer and winter dof is small when comparing these with spring and autumn dof in the cases of a 6-hourly and daily resolution. In these cases the ERA-40 and 20CR dof follow the same pattern of a peak in July, high values in winter and low values in other months. The fact that the July value exceeds the winter values is likely due to the fact that local processes (e.g. convection) dominate in summer, whereas in winter large teleconnection patterns are more prominent. This leads to more dof in summer as there are a larger number of principal trends (Wallace et al. 1993, Fraedrich et al 1995).

The studies mentioned above did not find these low dof values in spring and autumn. This is because these studies used monthly-averaged data and so calculated dof curves similar to those found in this research for such data. It seems that the atmospheric processes which cause such high values in July and the winter months operate on relatively short timescales and so do not register in monthly mean data.

That the dof in ERA-40 exceed those in the 20CR by the greatest margin in the summer months suggests that the 20CR represents large-scale processes better than it does small-scale ones. This is because small-scale processes are predominant in the summer while larger systems dominate the wintertime variability (Wallace et al. 1993, Fraedrich et al 1995). The reason for this difficulty in representing small-scale processes is almost certainly because of the smaller number of observations used in the 20CR compared to ERA-40. There are

enough observations that it includes the large-scale systems, but some of the smaller ones are not registered. Compo et al. (2006) performed a feasibility study for a 100 year reanalysis using only surface pressure observations with an EnSRF as a precursor to creating the 20CR. They predicted that the analysis would be less good in summer than in winter and it seems they were correct.

The same argument can be applied to why the 20CR and ERA-40 dof are most similar at a monthly resolution. Processes that operate on a small spatial scale will tend to also have a small temporal scale. Thus they will register in data at a 6-hourly or daily resolution but not in data that has a monthly resolution. This causes a greater difference in the dof between the two reanalyses at the higher temporal resolutions, since more processes are included in the ERA-40 data.

That the 20CR dof are closer to the ERA-40 dof for geopotential height than for temperature suggests that the 20CR represents geopotential height better than it does temperature. This tendency can also be seen in the chequerboard plots for the other varied parameters. Compo et al.'s (2006) feasibility study for the 20CR predicted that it would represent geopotential height very well and it seems that this is the case.

5.5 – Objective 3

5.5.1 – Latitude Bands

For the temperature results the same annual cycle as has been previously observed (maximum in July, high in winter, low in spring and autumn) can be seen for all latitude bands, most notably in the 60°-90°N band. This tells us that the processes which generate this pattern occur at all latitudes. For both variables the 60°-90°N band has considerably more dof than the others. This matches the results from the EOF plots in which the gridcells with the most extreme high and low loadings are located at high latitudes, suggesting that this is where most major activity occurs. For the geopotential height results there is far less annual variation than there was for the temperature results, also the annual cycle is different to that found for the whole NH. This suggests that there are different processes at different latitudes which together make up the cycle of annual variation previously observed.

The chequerboard plots (fig 4.4.1.3) for temperature show that dof for the 20CR most closely match those for ERA-40 in the tropics. This is also true, though to a lesser extent, in the plots for geopotential height. This is in contrast to the results of Anderson et al. (2005) who investigated the assimilation of surface pressure observations using an ensemble filter and found that 'for temperature in the middle of the atmosphere, the largest errors are found in the Tropics'. They however used an idealized global atmospheric prediction system and warn that their results will not necessarily apply to the real atmosphere. From the map showing locations of observation stations for the 20CR (fig 3.2.1.2) it can be seen that there are notably fewer stations at very high latitudes. ERA-40 is not so constrained by lack of observations since it has a much wider base of observations to draw on as it is not restricted

to just surface pressure readings. This is the most likely cause of the heightened margin between ERA-40 and 20CR dof for the 60°-90°N band.

5.5.2 – Zonal Regions

The ERA-40 plots show that the number of dof is very similar for different zonal regions. For the 20CR temperature data there is some disparity between the results from different zones; this is likely due to some areas having more observing stations than others. For instance, dof for the European region in the 20CR temperature data are quite similar to those for ERA-40, and the map showing locations of observation stations for the 20CR (fig 3.2.1.2) shows a very high concentration of stations in Europe. The USA also has a very high concentration of stations, but this is countered by the relatively small number in Canada as well as very few in the Pacific. Few observations in the Pacific means that the western side of this region will not be well represented as there is little information about incoming air masses. In contrast dof for the North Atlantic region for the 20CR match those in ERA-40 relatively well, despite the fact that there are relatively few observations there. This is because much information about air masses entering this region can be deduced from the high concentration of stations in the North American region.

5.5.3 - Pressure Levels

For the temperature results, the annual cycle for the lower levels (up to and including 500hPa) is the same as has been seen for previous plots at the 500hPa level. Above this level the pattern changes to simply having high values in summer and low in winter (for the most part). Hoinka (1998) states that the tropopause can lie anywhere between 100hPa and 400hPa, i.e. in the area where this change in the annual cycle occurs. This fits with the results since the stratosphere is much more stable than the troposphere and there are fewer circulation systems to transport heat (Wallace and Hobbs 2006); thus there is less month-by-month variation.

For temperature, the 1000hPa level has the fewest dof of those levels in the troposphere. This was the lowest level considered and as such the effect is likely due to the damping effect of the oceans, smoothing out the variations. Above this dof are similar up to the 500hPa level for the 20CR data, suggesting a lessening of this damping effect away from the surface. However, for the ERA-40 data the remaining tropospheric levels have similar numbers of dof and are exceeded by the 1000hPa level in July. This high July value for near-surface dof is likely due to the effect of increased solar forcing on boundary layer processes.

Fraedrich et al. (1995) considered height field data for the 300hPa, 500hPa and 1000hPa levels and found a tendency for dof to increase with height. This can be seen in the geopotential height results in this study (fig 4.4.3.2) from 850hPa to 500hPa. There are considerably fewer dof at 100hPa than at any other level; this is likely due to the comparative stability of the stratosphere when compared with the troposphere, as described above.

Manabe and Mahlman (1976) state that seasonal temperature variations in the lower stratosphere are 'essentially controlled by dynamical effects rather than by the seasonal variation of local heating due to solar radiation'. This suggests that the lower stratospheric levels will have more dof than higher levels as they are affected by additional processes. Thus it seems likely that calculating dof for higher levels would produce even lower results.

The results for geopotential height at the 250hPa level show a large amount of seasonal variation and in the same annual cycle as has previously been noted (very high in July, medium values in winter, low in spring and autumn) for the 20CR. For ERA-40 the cycle is simpler with higher values in summer than winter and a high peak in July. 250hPa lies between the polar front jet stream (300hPa) and the sub-tropical jet stream (200hPa) and as such can be used to obtain information about both (Weickmann & Chervin, 1988). Weickmann and Chervin (1988) investigated atmospheric seasonal cycles in global wind fields and noted that the jet streams had an annual cycle in which they intensified in winter and weakened in summer. This suggests that in winter the jet streams are dominating the variance (along with the large-scale teleconnection patterns already mentioned) and thus there are fewer dof. In summer these large-scale processes have less influence and so local patterns represent more of the variance, leading to more dof.

Temperature fluctuations are driven by pressure gradients; and so the fact that the 250hPa geopotential height dof results (fig 4.4.3.2) show a similar pattern to those previously found for temperature (fig 4.4.3.1) suggests that the jet stream annual cycle could be affecting that of temperature at lower levels. Weickmann and Chervin (1988) also identified a semi-annual cycle in atmospheric circulation which modulated the annual pattern, most notably in May

and November and in the tropics, sub-tropics and North Pacific. They were unable to give a definitive cause for this cycle though concluded that it was 'likely a combination of mechanisms including semi-annual equatorial convective forcing and semi-annual extratropical gradients'. This secondary cycle could be the reason for the low spring and autumn dof values found in this study, although in these results November values tend to be relatively high.

For the geopotential height results the margin by which ERA-40 dof exceed those for the 20CR increases with height. This is most likely because the 20CR uses only observations of surface pressure and the influence of a surface parameter will decrease with altitude (Uppala et al. 2004); thus the quality of the reanalysis will also decrease. In contrast ERA-40 uses data from many sources, such as radiosondes which can take in situ readings in the stratosphere itself.

5.6 – Objective 4

The Nef results show ERA-40 having the most dof, followed by HadSLP2 then the 20CR. They all have approximately the same annual cycle, with low values in winter, increasing numbers of dof from March through to May and a high value in September. That ERA-40 dof exceed HadSLP2 dof is to be expected given the wider range of observations available for the ERA-40 reanalysis. That HadSLP2 dof exceed 20CR dof can also be easily accounted for; especially given that the HadSLP2 dataset was incorporated into the International Surface Pressure Databank (Allan & Ansell 2006) which was used as the empirical input for the 20CR. The data assimilation process (as described in section 2.2) involves using the ensemble mean (equation [2.2.5]) and so inevitably a smoothing of the data ensues, removing some of the complexity and reducing the number of dof.

5.7 – Objective 5

For the January geopotential height plots the first six EOFs for the 20CR are very similar to those for ERA-40 (some have positive and negative values switched but the patterns are the same). EOF1 is similar to the Northern Annular Mode (NAM) teleconnections pattern:

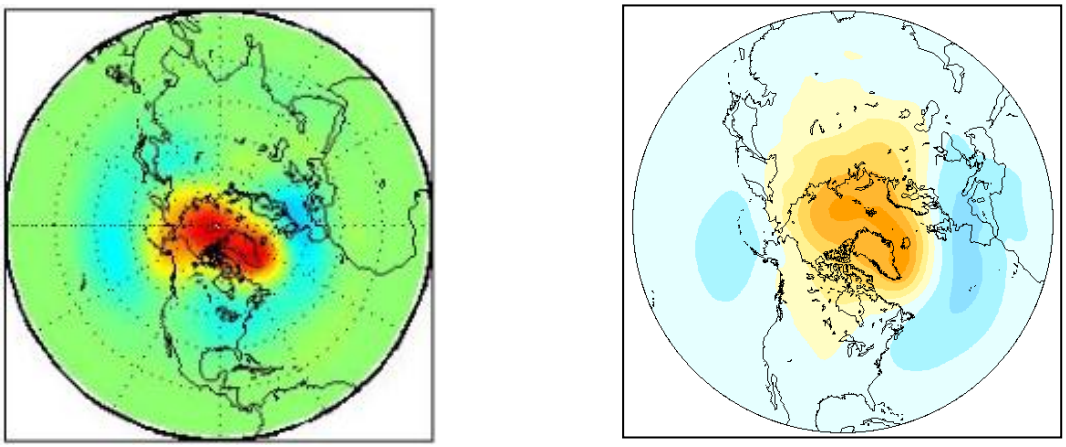

Fig 5.7.1: Left: EOF1 from 20CR January geopotential height data at 500hPa

Right: NAM for sea-level pressure, source: JISAO (2010)

Wallace et al. (2003) found that the NAO and the PNA teleconnections were dominant in wintertime. The NAM is related to the NAO and the PNA pattern can be seen incorporated in some of the other January EOF plots. For the July plots these patterns are not apparent and the areas of extreme high and low loadings are smaller (particularly in the ERA-40 plots), supporting what has previously been stated about local patterns dominating summertime variability.

The vast majority of the EOF plots have the centres of activity at very high latitudes. This matches what was previously found when comparing dof at different latitudes: the 60°-90°N

band had by far the most dof per unit area. Most major activity occurs at high latitudes and so this is where the dof are most concentrated.

The 20CR and ERA-40 EOF plots seem most similar for January and for geopotential height data. This affirms what had previously been found: that the two reanalyses most closely match in winter and that the 20CR represents geopotential height better than it does temperature. In general the two reanalyses match for the first two EOF's very well, but some differences start to appear beyond this. This is to be expected since even small changes can affect an EOF analysis so some degree of variation is anticipated.

Main Research Findings, Limitations & Conclusions

6.1 – Introduction

This chapter is divided into four main sections. Section 6.2 lists the main findings of this study, organised by objectives; section 6.3 gives limitations of this study; section 6.4 provides some suggestions for further research; and section 6.5 contains concluding remarks.

6.2 – Main Research Findings

6.2.1 - Objective 1

Dof were calculated on a decade-by-decade basis for each reanalysis dataset. It was found that the number of dof in the 20CR increased throughout the period; this was the case for both the whole NH and the NH extratropics. No trend was visible for the ERA-40 dof.

6.2.2 - Objective 2

Dof were calculated for both reanalyses at 6-hourly, daily and monthly resolutions. It was found that there was greater annual variation for temperature than for geopotential height, with temperature dof having an annual cycle of a peak in July, medium values in winter and low values in spring and autumn for the higher temporal resolutions. This cycle was not visible at a monthly resolution, nor for geopotential height dof. ERA-40 dof were generally higher than those for the 20CR, with the greatest difference being in the summer months. This is attributed to the 20CR having more difficulty representing the local processes which dominate summertime variability than the large-scale dynamics which are predominant in wintertime. 20CR dof were closer to those of ERA-40 for geopotential height than for

temperature, suggesting that the 20CR represents geopotential height better than it does temperature.

6.2.3 - Objective 3

Dof were calculated for both reanalyses for different latitude bands, zonal regions and pressure levels. It was found that there are the greatest numbers of dof at high latitudes; this is also the area in which the 20CR is poorest, the difference between its dof and those of ERA-40 being greatest here. ERA-40 results showed that there is little difference in the number of dof for different zonal regions. The 20CR represented the European and North Atlantic regions most accurately, with the greatest disparity between dof for the two reanalyses being in the North Pacific region. When calculating dof for different pressure levels it was found that there is more annual variability for temperature in the troposphere than in the stratosphere. Also, for geopotential height, dof tend to increase with altitude in the troposphere. Geopotential height dof around the level of the jet-streams show a large amount of annual variability and this may drive the observed temperature dof cycle seen at lower levels. For geopotential height, the quality of the 20CR tended to decrease with altitude, though this was not apparent in the temperature results.

6.2.4 - Objective 4

Dof were calculated for each reanalysis and for the HadSLP2 gridded SLP dataset on a monthly basis. It was found that ERA-40 had the most dof, followed by HadSLP2 and then the 20CR.

6.2.5 - Objective 5

The first six EOFs for each reanalysis for both variables and for both January and July were plotted. These reaffirmed previous results that the variance is concentrated at high latitudes and that large-scale dynamics are dominant in winter but are less prominent in the summer months. The first few EOFs are very similar for both reanalyses, particularly in January and for geopotential height, confirming that this is where the 20CR performs the best.

6.3 - Limitations

One of the main limitations of this study is that by comparing the 20CR with ERA-40, only the period where they overlap is used, and this is just 44 years compared to the 138 years which the 20CR covers. As such this study does not assess the quality of the whole 20CR, merely the period from 1958 to 2001.

The discussion of the results found in this study is in some ways incomplete as not all the trends could be accounted for; for instance the cause of the low numbers of dof in spring and autumn. A justification for this would require a thorough breakdown of atmospheric dynamics and such an in depth analysis was not within the purview of this study.

6.4 - Suggestions for Further Research

In this study temperature and geopotential height data were analysed and it was found that the 20CR represents geopotential height better than it does temperature. It would be interesting to perform the same analysis for other variables to see how well they compare.

Two datasets having comparable numbers of dof tells us that they have a similar level of complexity, but not that the complexity is distributed in the same way. As such alternative validation methods could be used (e.g. root-mean-square error or anomaly correlation) to ascertain how similar the actual values are to each other. A close match here as well as similar dof would be solid evidence of two datasets being closely related.

6.5 - Conclusion

This research should be of use to anyone wishing to make use of the 20CR. It provides information as to where it is most accurate and where it should be used with caution, and the comparisons with ERA-40 and HadSLP2 inform users which dataset would be most beneficial for their circumstances. It also provides useful information for anyone working with dof. The annual cycle of a peak in July, medium values in winter and low values in spring and autumn to the author's knowledge has not been found before; and while no definitive cause could be given in this study it is hoped that future research will provide a justification for this pattern. The variations of dof with latitude, zonal region, etc. provide new information as to the nature of atmospheric dynamics and it is hoped that this will lead to a deeper understanding of the atmosphere as a whole.

Bibliography

Allan, R. J. and Ansell, T. J., 2006. A new globally complete monthly historical mean sea level pressure data set (HadSLP2): 1850-2004. *American Meteorological Society: Journal of Climate*, [Online] 19(22), p. 5816-5842. Available at: http://journals.ametsoc.org/loi/clim (AMS Journals Online) [Accessed 16 August 2010]

Anderson, J., Wyman, B., Zhang, S. and Hoar, T., 2005. Assimilation of Surface Pressure Observations using an Ensemble Filter in an Idealized Global Atmospheric Prediction System. *American Meteorological Society: Journal of the Atmospheric Sciences*, [Online] 62 (8), p. 2925-2938. Available at: http://journals.ametsoc.org/doi/pdf/10.1175/JAS3510.1 (AMS Journals Online) [Accessed 11 June 2010]

Bengtsoon, L, Hagemann, S. and Hodges, K., 2004. Can Climate Trends be Calculated from Reanalysis Data? *Journal of Geophysical Research*, 109(11). Available at: http://www.agu.org/journals/jd/ (American Geophysical Union) [Accessed 6 July 2010]

Bretherton, C., Widmann, M., Dymnikov, V., Wallace, J. and Bladé, I., 1999. The Effective Number of Spatial Degrees of Freedom of a Time-Varying Field. *American Meteorological Society: Journal of Climate*, [Online] 12(7), p. 1990-2009. Available at: http://journals.ametsoc.org/loi/clim (AMS Journals Online) [Accessed 27 July 2010]

Compo, G., Whitaker, J. and Sardeshmukh, P., 2006. Feasibility of a 100-Year Reanalysis using only Surface Pressure Data. *Bulletin of the American Meteorological Society*, [Online] 87 (2), p. 175-190. Available at: http://journals.ametsoc.org/doi/pdf/10.1175/BAMS-87-2-175 (AMS Journals Online) [Accessed 14 June 2010]

Compo, G., Whitaker, J. and Sardeshmukh, P., 2008. The 20th Century Reanalysis Project. In WCRP, *Proceedings of the Third WCRP International Conference on Reanalysis*, The University of Tokyo, Japan, 28 January – 1 February 2008

Fraedrich, K., Ziehmann, C. and Sielmann, F., 1995. Estimates of Spatial Degrees of Freedom. *Journal of Climate*, 8(2), p. 361-369

Hamill, T. and Whitaker, J., 2001. Distance-Dependent Filtering of Background Error Covariance Estimates in an Ensemble Kalman Filter. *American Meteorological Society: Monthly Weather Review*, [Online] 129 (11), p. 2776-2790. http://www.ametsoc.org/pubs/journals/mwr/ (AMS Journals Online) [Accessed 15 June 2010]

Hazelrigg, L., 2004. Inference. In Hardy, M. and Bryman, A., eds. *Handbook of Data Analysis*. Sage, 2004. Ch.4

Hoinka, K., 1998. Statistics of Global Tropopause Pressure. *American Meteorological Society: Monthly Weather Review*, [Online] 126(12), p. 3303-3325. Available at:

http://www.ametsoc.org/pubs/journals/mwr/ (AMS Journals Online) [Accessed 30 August 2010]

JISAO [Joint Institute for the Study of the Atmosphere and Ocean], 2010. *Northern Annular Mode (NAM) and Pacific / North American (PNA) pattern monthly and daily indices for 1948 - March 2010*, [Online] (Updated May 2010) Available at: http://jisao.washington.edu/analyses0302/ [Accessed 1 September 2010]

Livezey, R. and Chen, W., 1983. Statistical Field Significance and its Determination by Monte Carlo Techniques. *American Meteorological Society: Monthly Weather Review*, [Online] 111(1), p .46-59. Available at: http://www.ametsoc.org/pubs/journals/mwr/ (AMS Journals Online) [Accessed 27 July 2010]

Lorenz, E., 1969. Atmospheric Predictability as Revealed by Naturally Occurring Analogues. *American Meteorological Society: Journal of the Atmospheric Sciences*, [Online] 26(4), p. 636-646. Available at http://journals.ametsoc.org/loi/atsc (AMS Journals Online) [Accessed 27 July 2010]

Ma, L., Zhang, T., Li, Q., Frauenfeld, O. and Qin, D., 2008. Evaluation of ERA-40, NCEP-1, and NCEP-2 reanalysis air temperatures with ground-based measurements in China. *Journal of Geophysical Research: Atmospheres*, [Online] 113. Available at: http://www.agu.org/journals/jd/ (American Geophysical Union) [Accessed 30 June 2010]

Manabe, S. and Mahlman, J., 1976. Simulation of Seasonal and Interhemispheric Variations in the Stratospheric Circulation. *American Meteorological Society: Journal of the Atmospheric Sciences*, [Online] 33(11), p. 2185-2217. Available at: http://journals.ametsoc.org/doi/abs/10.1175/1520-0469%281976%29033%3C2185%3ASOSAIV%3E2.0.CO%3B2 (AMS Journals Online) [Accessed 31 August 2010]

NOAA [National Oceanic and Atmospheric Administration], 2010. *Twentieth Century Reanalysis (V2): Summary*. [Online] Available at: http://www.esrl.noaa.gov/psd/data/gridded/data.20thC_ReanV2.html [Accessed 16/08/10]

Plougonven, R., Teitelbaum, H. and Zeitlen, V., 2003. Inertia gravity wave generation by the tropospheric midlatitude jet as given by the Fronts and Atlantic Storm-Track Experiment radio soundings. *Journal of Geophysical Research: Atmospheres*, [Online] 108(21). Available at: http://www.agu.org/journals/jd/ (American Geophysical Union) [Accessed 4 August 2010]

Santer, B. et al., 2004. Identification of anthropogenic climate change using a second-generation reanalysis, *Journal of Geophysical Research: Atmospheres*, [Online] 109(24). Available at: http://www.agu.org/journals/jd/ (American Geophysical Union) [Accessed 6 July 2010]

Swanson, K. and Pierrehumbert, R., 1997. Lower tropospheric heat transport in the Pacific storm track. *American Meteorological Society: Journal of the Atmospheric*

Sciences, [Online] 54(11), p. 1533-1543. Available at: http://journals.ametsoc.org/loi/atsc (AMS Journals Online) [Accessed 4 August 2010]

Talagrand, O., 1997. Assimilation of Observations, an Introduction. *Journal of the Meteorological Society of Japan*, [Online] 75 (1B), p. 191-209. Available at: http://www.journalarchive.jst.go.jp/jnlpdf.php?cdjournal=jmsj1965&cdvol=75&noissue=1B&startpage=191&lang=en&from=jnltoc (Journal@rchive) [Accessed 15 June 2010]

Toth, Z., 1995. Degrees of freedom in Northern Hemisphere circulation data. *Tellus Series A: Dynamic meteorology and oceanography*, 47(4), p. 457-472

Uppala, S., Kållberg, P., Hernandez, A., Saarinen, S., Fiorino, M., Li, X., Onogi, K., Sokka, N., Andrae, U. and Bechtold, V., 2004. ERA-40: ECMWF 45-year reanalysis of the global atmosphere and surface conditions 1957–2002. *ECMWF Newsletter*, [Online] 101, pp.2-21. Available at: http://www.ecmwf.int/publications/newsletters/pdf/101.pdf (ECMWF) [Accessed 4 July 2010]

Uppala. S et al., 2005. The ERA-40 Re-analysis. *Quarterly Journal of the Royal Meteorological Society*, [Online] 131(612), p. 2961-3012. Available at: http://onlinelibrary.wiley.com/journal/10.1002/%28ISSN%291477-870X (Wiley Online Library) [Accessed 29 June 2010]

Van Den Dool, H. and Chervin, R., 1986. A Comparison of Month-to-Month Persistence of Anomalies in a General Circulation Model and in the Earth's Atmosphere. *American Meteorological Society: Journal of the Atmospheric Sciences*, [Online] 43(14), p. 1454-1466. Available at: http://journals.ametsoc.org/loi/atsc (AMS Journals Online) [Accessed 28 July 2010]

Wallace, J., Zhang, Y. and Lau, K., 1993. Structure and seasonality of interannual and interdecadal variability of the geopotential height and temperature fields in the Northern Hemisphere troposphere. *American Meteorological Society: Journal of Climate*, [Online] 6(11), p. 2063-2082. Available at: http://journals.ametsoc.org/loi/clim (AMS Journals Online) [Accessed 27 August 2010]

Wallace, J. and Hobbs, P., 2006. *Atmospheric Science*. 2nd ed. Academic Press

Wang, X. and Shen, S, 1999. Estimation of Spatial Degrees of Freedom of a Climate Field. *American Meteorological Society: Journal of Climate*, [Online] 12(5), p. 1280-1291. Available at: http://journals.ametsoc.org/loi/clim (AMS Journals Online) [Accessed 27.July 2010]

Weickmann, K. and Chervin, R., 1988. The Observed and Simulated Atmospheric Seasonal Cycle. Part 1: Global Wind Field Modes. *American Meteorological Society: Journal of Climate*, [Online] 1(3), p. 265-289. Available at: http://journals.ametsoc.org/doi/pdf/10.1175/1520-

0442%281988%29001%3C0265%3ATOASAS%3E2.0.CO%3B2 (AMS Journals Online) [Accessed 2 September 2010]

Whitaker, J. and Hamill, T., 2002. Ensemble Data Assimilation without Perturbed Observations. *American Meteorological Society: Monthly Weather Review*, [Online] 130 (7), p. 1913-1924. Available at: http://www.ametsoc.org/pubs/journals/mwr/ (AMS Journals Online) [Accessed 14 June 2010]

Whitaker, J., Compo, G., Wei, X. and Hamill, T., 2004. Reanalysis without Radiosondes using Ensemble Data Assimilation. *American Meteorological Society: Monthly Weather Review*, [Online] 132 (5), p. 1190-1200. Available athttp://www.ametsoc.org/pubs/journals/mwr/ (AMS Journals Online) [Accessed 14 June 2010]

Widmann, M., 2010. Statistics, M3. [Lecture notes] *Methods for finding coupled patterns in two data sets*. Atmospheric Data Processing and Statistics. University of Birmingham, GEES 112, February.

Yin, X., Gleason, B., Compo, G., Matsui, N. and Vose, R., 2008. The International Surface Pressure Databank (ISPD) land component version 2.2. *National Climatic Data Center*, [Online] Asheville, NC, p. 1-12. Available at: ftp://ftp.ncdc.noaa.gov/pub/data/ispd/doc/ISPD2_2.pdf [Accessed 16/08/10]

Appendices

APPENDIX 1

DERIVATION OF BRETHERTON ET AL.'S (1999) DOF FORMULAE

Bretherton et al. (1999) define the dof N^* of a time-varying spatial field $\psi(t)$ as 'the number of uncorrelated random normal variables a_k, each having zero mean and the same population variance $\langle a^2 \rangle$, for which the χ^2 distribution for the specified functional $[\sum_{i=1}^{N} \psi_i^2(t)$, N is number of stations] most closely matches the PDF [probability density function] of the functional of $\psi(t)$.'

Bretherton et al. (1999) devised two formulae for the calculation of the effective number of spatial degrees of freedom (ESDOF). They first define the following variable at time t:

$$E(t) \coloneqq \sum_{i=1}^{N} \psi_i^2(t) \qquad \textbf{[A1.1]}$$

Where N is the number of stations and $\psi_i(t)$ is the anomaly from the mean of station i at time t. For the first formula they cite Bagrov's (1969) work in requiring that 'the χ^2 distribution match the observed distribution's ensemble mean value $\langle E \rangle$ and its temporal variance of E about the ensemble mean'. This leads this formula to be known as a 'moment matching' estimate for the degrees of freedom, since mean and variance are the first two statistical moments respectively. For a χ^2 distribution, $\langle E \rangle = N^* \langle a^2 \rangle$ and $\mathrm{var}(E) = 2N^* \langle a^2 \rangle^2$, where N^* and $\langle a^2 \rangle$ are as described above. Solving for N^* gives the moment matching estimate for dof:

$$N^*_{mm} = \frac{2\langle E \rangle^2}{var(E)}, \text{ where } \langle a^2 \rangle_{mm} = \frac{var(E)}{2\langle E \rangle} \qquad \textbf{[A1.2]}$$

(Bretherton et al. 1999)

Their second formula involves finding the eigenvalues λ_k of the $N \times N$ covariance matrix of the ψ_i's. This assumes that that the ψ_i's are normally distributed and that the covariance matrix is known with sufficient accuracy. It can be shown that:

$$\langle E \rangle = \sum_{k=1}^{N} \lambda_k \quad \textbf{[A1.3]}$$

$$var(E) = 2 \sum_{k=1}^{N} \lambda_k^2 \quad \textbf{[A1.4]}$$

Substituting these into [A1.2] gives an *eigenvalue formula* for the degrees of freedom:

$$N_{ef}^{*} = \frac{\left(\sum_{k=1}^{N} \lambda_k\right)^2}{\sum_{k=1}^{N} \lambda_k^2} \quad \textbf{[A1.5]}$$

(Bretherton et al. 1999)

APPENDIX 2

LOCATIONS OF DATA & MATLAB PROGRAMS

All programs were run on the computer 'cloud' in the department of Geography, Earth & Environmental Sciences, University of Birmingham, UK.

20th Century Reanalysis

Data and programs can be found in /data/snow3/med933/20thC_ReanV2

Air temperature data is in files: air.[year].nc

Geopotential height data is in files: hgt.[year].nc

Read and regrid data: regridtest.m

Save regridded data in separate files: postregrid.m

Calculate decadal dof: dof_dec.m

Calculate dof for 6-hourly data: dof_6hourly.m

Calculate dof for daily data: dof_daily.m

Calculate dof for monthly data: dof_monthly.m

Calculate dof for different latitude bands: dof_lat.m

Calculate dof for different zonal regions: dof_zonal.m

Calculate dof for different pressure levels (includes reading and regridding data): dof_levels.m

Calculate dof at 1000hPa on a 5 degree grid (includes reading and regridding data): dof_1000_5.m

Plot first 6 EOFs: EOF.m

ERA-40

Data and programs can be found in /data/snow3/med933/ERA40/netcdf

Data is in files: liap[year]_zt.nc

Some data is missing:

1969	2nd timestep 13/08 – 4th timestep 31/08
1998	3rd timestep 12/11 – 4th timestep 30/11
2001	1st timestep 12/09 – 4th timestep 30/09 3rd timestep 17/10 – 4th timestep 31/10

500hPa data for these periods is contained in the files: missing[year]_500.nc

And for other pressure levels: missing[year].nc

It is necessary to use a scale factor and add an offset when using this data, details of which are provided in these files.

Read data and save to separate files: Eread_lat.m & Eread_equator.m

Concatenate saved data: Edata_cat.m (for temperature data) & Edata_cat_hgt.m (for geopotential height data)

Calculate decadal dof: Edof_dec.m

Calculate dof for 6-hourly data: Edof_6hourlytest.m

Calculate dof for daily data: Edof_daily.m

Calculate dof for monthly data: Edof_monthly.m

Calculate dof for different latitude bands: Edof_lat.m

Calculate dof for different zonal regions: Edof_Eur.m

Calculate dof for different pressure levels (includes reading data): Edof_levels.m (temperature) & Ehgtdof_levels.m (geopotential height)

Calculate dof at 1000hPa on a 5 degree grid (includes reading and regridding data): Edof_1000_5.m

Plot first 6 EOFs: EEOF.m

HadSLP2

Data and programs can be found in /data/snow3/med933/gridded_data

Data is in file: hadslp2.asc

FORTRAN code to read data (provided by www.hadobs.org): hadslp2.f

Calculate dof from hadslp2.f output: hadslp2.m